Alkoxide complexes of rhenium - precursors of nanomaterials

Olesya A. Nikonova

Faculty of Natural Resources and Agricultural Sciences
Department of Chemistry
Uppsala

Doctoral Thesis
Swedish University of Agricultural Sciences
Uppsala 2011

Cover: Nanobeads of mixed oxide based on $TaNbReO_x$
    (photo: O. Nikonova)

Alkoxide complexes of rhenium - precursors of nanomaterials

Abstract

The thesis presents the work constituted by two major parts: (1) − synthesis of new mono-, bi- and trimetallic complexes based on Re, Nb and Ta and their physical-chemical characterization, and (2) − preparation of nanostructural functional materials derived from these complexes. The precursors and materials were characterized by FTIR, NMR, MS, SEM−EDS, TEM and X-ray diffraction.

The electrochemical method and the interaction of Re_2O_7 with $M_2(OR)_{10}$ ($M = Nb$ or/and Ta) were used to obtain $Re_4O_4(OEt)_{12}$ and $(M_{1-x}M'_x)_4O_2(OR)_{14}(ReO_4)_2$ ($M = Nb; M' = Ta; R = Me, Et, {}^nPr$), where x = 0–1, respectively. The structures of these complexes were determined by single-crystal X-ray diffraction. The influence of the increasing ligand size on the solubility and stability of the complexes $Re_4O_4(OEt)_{12}$ and $(M_{1-x}M'_x)_4O_2(OR)_{14}(ReO_4)_2$ ($M = Nb, M' = Ta; R = Me, Et, {}^nPr$) has been established.

Nanosized Re metal particles (approximately 3 nm in diameter) were obtained from $Re_4O_4(OEt)_{12}$ by thermal decomposition in inert atmosphere at as low temperature as 380°C. Semi-ordered macro porous monoliths with the pore size in the range 100–250 nm, with the crystal structure related to the γ-Ta_2O_5, were produced from $(Nb_{1-x}Ta_x)_4O_2(OMe)_{14}(ReO_4)_2$ ($x=0.3, 0.5, 0.7$) via thermal decomposition in air at the temperatures ≤ 1000°C, while in dry nitrogen the α-Nb_2O_5 for the Nb-rich precursors and γ-Ta_2O_5 for Ta:Nb ≥ 1:1 at the temperatures ≤ 1000°C were formed.

The $Re_4O_4(OEt)_{12}$ and $Ta_4O_2(OEt)_{14}(ReO_4)_2$ alkoxide complexes have been used as precursors for Re oxide based catalysts. The simultaneous presence of the chemically connected oxidative (perrhenate) and acidic (tantalum oxide) components in the catalyst permit one-step production of DMM.

The hydrolysis of $(M_{1-x}M'_x)_4O_2(OEt)_{14}(ReO_4)_2$ ($M = Nb; M' = Ta; x=0–1$) leads to formation of nanostaructural materials (nanobeads). The particles remain amorphous and retain Re until rather high temperatures (700°C). The Re content is lost at 1000°C with formation of porous nanobeads with crystal structure related to the γ-Ta_2O_5 and α-Nb_2O_5 for the corresponding precursors.

Keywords: alkoxide, nanomaterials, semi-ordered macro porous materials, catalyst, nanobeads, single-crystal X-ray diffraction, SEM, TEM.

Author's address: Olesya A. Nikonova, SLU, Department of Chemistry,
P.O. Box 7015, 750 07 Uppsala, Sweden
E-mail: Olesya.Nikonova@slu.se

Dedication

To my family

"I think that a particle must have a separate reality, depending on the measurement method ... I like to think that the moon is there even when I am not looking at it ..."

A. Einstein

Contents

List of Publications

This thesis is based on the work contained in the following papers, referred to by Roman numerals in the text:

I   Nikonova O.A., Jansson K., Kessler V. G., Sundberg M., Baranov A.I., Shevelkov A.V., Drobot D.V., Seisenbaeva G. A. (2008). Electrochemical Synthesis, Structural Characterization and Decomposition of Rhenium Oxoethoxide, $Re_4O_4(OEt)_{12}$. Ligand Influence on the Structure and Bonding in the High–Valent Tetranuclear Planar Rhenium Alkoxide Clusters. *Inorganic Chemistry* 47, 1295-1300.

II Nikonova O.A., Kessler V.G., Seisenbaeva G.A., Drobot D.V., Shcheglov P.A. (2007). Synthesis and X-ray Single Crystal Study of Niobium and Tantalum Oxo-Ethoxo-Perrhenates $M_4O_2(OEt)_{14}(ReO_4)_2$. *Polyhedron* 26(4), 862-866.

III Nikonova O.A., Seisenbaeva G.A., Kessler V.G., Shcheglov P.A., Drobot D.V. (2007). Comparative Study of Bimetal Alkoxo Complexes of Rhenium, Niobium and Tantalum by Single-Crystal X-ray Diffraction and IR Spectroscopy. *Russian Journal of Inorganic Chemistry* 52(11), 1687–1692.

IV Nikonova O.A., Kessler V.G., Seisenbaeva G.A. (2008). Substitution Features in the Isomorphous Replacement Series for Metal-Organic Compounds $(Nb_xTa_{1-x})_4O_2(OMe)_{14}(ReO_4)_2$, x = 0.7, 0.5, 0.3—Single-Source Precursors of Complex Oxides with Organized Porosity. *Journal of Solid State Chemistry* 181(12), 3294-3302.

V Nikonova O.A., Capron M., Fang G., Faye J., Mamede A.-S., Jalowiecki-Duhamel L., Dumeignil F., Seisenbaeva G.A. (2011) Novel approach to rhenium oxide catalysts for selective oxidation of methanol to DMM. *Journal of Catalysis*, accepted, *in press*.

VI Nikonova O.A., Kessler V.G., Seisenbaeva G.A. Morphology and crystallinity control of early transition metal complex oxide nanobeads. *Manuscript*.

Related article, not included in the thesis

VII Drobot D.V., Seisenbaeva G.A., Kessler V.G., Shcheglov P.A., Nikonova O.A., Mihnevich S.N., Petrakova O.A. (2009) Cluster and Heterometallic Alkoxide Derivatives of Rhenium and d-Elements of V–VI Groups. *Journal of Cluster Science* 20(1), 23–36

Papers I–V are reproduced with the permission of the publishers.

The contribution of Nikonova O.A. to the papers included in this thesis was as follows:

I   Synthesis of the precursor, performing FTIR and TGA analysis, characterization of the decomposition product by XPD analysis, discussion and writing of the manuscript;

II Synthesis of bimetallic complexes, characterization them by FTIR spectroscopy, discussion and writing of the manuscript.

III Synthesis of bimetallic complexes, investigation of solubility, analysis of IR spectra and crystallographic structure data refinement, discussion and writing the article.

IV Synthesis of trimetallic complexes, their characterization by MS, FTIR, SEM-EDS and X-ray powder diffraction analysis, performing TGA analysis in two different atmospheres and characterization of the thermal treated products by XPD and SEM-EDS analysis, structure refinement based on the XPD results. Discussion and writing of the manuscript.

V   Synthesis of precursors and preparation of catalysts, analysing them by FTIR, XPD, SEM-EDS and HRTEM. Discussion and writing of the manuscript. Corresponding author of this article.

VI Synthesis of bi- and trimetallic complexes and preparation of nanobeads from them. Performing TGA. Characterization by FTIR, XPD and SEM-EDS analysis. Discussion and writing of the manuscript.

10

1 Introduction

The research within this thesis is focused on the synthesis and characterization of a new family of mono-, bi- and trimetallic complexes on the basis of rhenium, niobium and tantalum, and on production from them of nanostructural and porous functional materials for applications in catalysis.

1.1 Application of Rhenium, Niobium and Tantalum and their compounds

1.1.1 Rhenium

Rhenium and its compounds such as sulphides, oxides, alloys and carbonyl complexes have found application as catalysts in petroleum production, different organic syntheses and radiotherapy.

Rhenium metal is broadly used as a component of catalysts for alkylation in organic synthesis and for industrial processes such as reforming of petroleum feedstock and metathesis of alkenes (Guryev *et al.*, 2007; Mol, 2004; Xiao & Puddephatt, 1995). These catalysts have shown good activity in the hydrocarbon cracking and selective hydrogenation, hydrodesulphurization of heavy crude oil and also selective dehydroaromatization of methane and ethane to benzene (Laurenti *et al.*, 2008; Escalona *et al.*, 2007; Shu *et al.*, 2003; Wang *et al.*, 2003; Escalona *et al.*, 2002; Räty & Pakkanen, 2000; Wang *et al.*, 2000; Okal & Kubicka, 1998). Moreover, Re-containing catalysts show high performance for selective oxidation of methanol and ethanol (Tsoncheva *et al.*, 2007; Chang *et al.*, 2004; Yuan *et al.*, 2000b). Recently, it was discovered that Rhenium/zeolite catalyst is very active in the selective oxidation of benzene to phenol (Kusakari *et al.*, 2004).

Rhenium heptoxide, Re_2O_7, has shown high catalytic activity in olefin metathesis and is the only catalyst, which can work efficiently at room

temperature (Salameh et al., 2008). Moreover, this heterogeneous catalyst can also be used to convert oleate esters when activated by organic derivates of Tin, which use, however, is detrimental to the regeneration process (Mol, 2004). Re_2O_7 dispersed on mesoporous alumina (abbreviated as meso-Al_2O_3) with a narrow pore-size distribution centered at 3 nm has shown higher catalytic activity in the metathesis of internal as well as terminal olefins without functional groups than Re_2O_7 on common γ–Al_2O_3 in liquid phase (Bakala et al., 2008; Onaka & Oikawa, 2002). Rhenium oxide supported on ordered mesoporous alumina has even been claimed as more active and selective catalyst than Re_2O_7/ γ–Al_2O_3 for alkene metathesis (Oikawa et al., 2004).

The most efficient catalyst based on Rhenium is the well-known methyltrioxorhenium (CH_3ReO_3, MTO). This catalyst is particularly useful in oxidation chemistry and shows high activity for epoxidations, C–H and Si–H oxidations, but it can also be applied in other types of catalytic reactions such as olefin metathesis and aldehyde olefinations (Jain & Kühn, 2007; Salameh et al., 2007; Mandelli et al., 2001; Buffon et al., 1992a; Buffon et al., 1992b).

Rhenium complexes, in particular, of the type fac-$[Re(L)(CO)_3Cl]$ (where L is a bidentate ligand such as 2,2'-bipyridyl or two monodentate ligands such as 4,4'-bipyridyl), was used as heterogeneous catalyst in the reduction of CO_2 (Chen et al., 2009; Cecchet et al., 2006; Scheiring et al., 1997). Furthermore, complexes with common core fac-$[Re(L)(CO)_3]$ configuration, where L is a ligand, are used in radio pharmacology as analogs to fac-$[99mTc(L)(CO)_3]$-based radiopharmaceuticals (Anaya et al., 2008; Christoforou et al., 2007).

Rhenium and Molybdenum oxo-methoxide complexes $Re_2O_3(OMe)_6$, $ReMoO_2(OMe)_7$ and $MoO_2(OMe)_8$ are used as precursors to prepare highly dispersed mono- and bimetallic oxide species, which were supported on the micro porous NaY zeolite and mesoporous SiO_2 and Al_2O_3. It should be mentioned, that oxomethoxo-complexes of Re and Mo lost their ligands when loaded into the micro porous NaY zeolite, so that just metal sub-oxide cores, ReO_3 and MoO_3, remain in the intracrystalline voids and reside there as nanosized particles. The obtained clusters reveal both acidic and redox properties (Kusakari et al., 2004; Kustov et al., 2004b).

Recently it was shown that ReO_x-containing catalysts on a number of supports provide high catalytic activity and selectivity in certain conditions for partial oxidation of methanol to methylal (DMM) (Chang et al., 2004; Yuan & Iwasawa, 2002; Yuan et al., 2000a; Yuan et al., 2000b). Numerous studies have revealed that methanol oxidation is very sensitive to the nature

12

of active sites and can be used to study the acidic and oxidation properties of catalytic surfaces (Briand *et al.*, 2000; Tatibouët, 1997; Matsuoka *et al.*, 1990). The process of methanol oxidation leads to step-wise formation of formaldehyde (F), formic acid (FA) and finally CO_2. If the catalyst also has acidic properties, then the aforementioned products can react through a dehydration/condensation reaction with methanol to produce dimethylether (DME), dimethoxymethane (DMM) and finally methylformate (MF) (*see Fig. 1*).
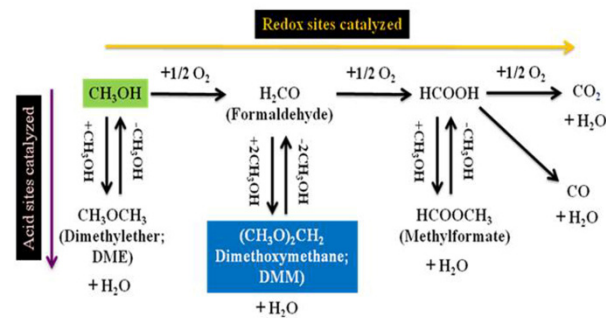
Figure 1. Scheme of oxidation / dehydration methanol

The most interesting product for industry is DMM, which possesses a high degree of chemical stability, while the absence of carbon-carbon bonds makes this compound a good candidate as a fuel additive. Industrially, methylal is produced by two-stage processes: methanol oxidation to formaldehyde on silver and ferric molybdate catalysts and dehydrative condensation of the formaldehyde with methanol catalyzed by sulfuric acid. Thus, DMM production patents are rather scarce because of the difficulty of obtaining a high yield in DMM in one step. Different catalytic systems have been studied in oxidation of methanol into DMM such as $VO_x - TiO_2$ (Guo *et al.*, 2010; Liu & Chang, 2000), V_2O_5-TiO_2/SO_4^{2-} (Zhao *et al.*, 2010), Mo supported catalysts (Brandhorst *et al.*, 2006), FeMo based catalysts (Gornay *et*

al., 2010). Among these catalysts, it has been shown that ReO_x based catalysts provide high activity and selectivity toward DMM in certain conditions (Secordel *et al.*, 2010; Yuan *et al.*, 2000b) e.g. low conversion of methanol.

1.1.2 Niobium and Tanatalum

Niobium and Niobium-based compounds find many technological applications, for instance, as oxygen sensors (Rosenfield *et al.*, 1996), waveguides (Saito Ya. *et al.*, 1992), or as tunnel barriers in Josephson tunnel junctions (Halbritter, 1987). Niobium has an excellent corrosion resistance in mineral acids at ambient conditions, except in hydrofluoric acid, but in extremely corrosive media, like concentrated acids and/or at high temperature, Niobium is appreciably attacked. On the contrary, Tantalum is practically unaffected in all acidic solutions, even concentrated and hot (Robin & Rosa, 2000). Alloys of these two metals with such metals as Ni and Re, provide most corrosion resistive materials (Mugishima *et al.*, 2006; Vinet *et al.*, 2003; Liu & Chang, 2000; Cui & Jin, 1999). There are a significant number of Niobium-based materials, for example, $NbCl_5$, NbF_5, NbH_x, NbS_2, NbN, NbC, NbO_x and Nb organometallic compounds which are effective catalysts for many reactions (Tanabe, 2003). Recently, it was found out that $TaCl_5$ and $Ta(OEt)_5$ are good catalysts for selective synthesis of sulfoxides and sulfones (Kirihara *et al.*, 2009). The Niobium oxide coated mesoporous materials as well as Tantalum oxide supported on different mesoporous molecular sieves have found broad application as catalysts for oxidation of methanol (Feliczak *et al.*, 2009; Sobczac *et al.*, 2008), for the synthesis of vegetable oil-based products (Jehng *et al.*, 2007), for propene epoxidation (Held & Florczak, 2009) and showed very high selectivity in formaldehyde production from methanol (Trejda *et al.*, 2008).

The pentoxides of Niobium and Tantalum, Nb_2O_5 and Ta_2O_5, are used in optical applications as high index and low loss materials for optical waveguides, interference filters, anti–reflective coating (for example in solar cells) (Masse *et al.*, 2006).

Niobium and Tantalum oxides have been reported to remarkably enhance catalytic activity and selectivity and to prolong catalytic life, when a small amount of the oxides was added to known catalysts (Ushikubo, 2000). Application of Niobium and Tantalum oxides as matrices in the *in situ* synthesis of Rhenium oxide-based nanocomposites can offer a cost–efficient approach to materials with enhanced stability to reduction. In the literature, there are publications on Rhenium-based catalysts for the metathesis of olefins CH_3ReO_3/Nb_2O_5 (Buffon *et al.*, 1997; Buffon *et al.*, 1992a; Buffon *et*

al., 1992b), which showed high catalytic activity for metathesis of 1–pentene (Buffon *et al.*, 1992b). Tantalum pentoxide has also found broad application as oxide support. The redox activity and selectivity of various surface metal oxides such as Re_2O_7, Nb_2O_5, WO_3, MoO_3 on Ta_2O_5 reflect the natural redox properties of these pure metal oxides and the more active surface redox sites minimized the contribution from the surface acidic sites of the Ta_2O_5 support (Chen *et al.*, 2003). Tantalum composite catalyst has also been used for esterification reaction of laurilic acid with ethanol, an important pre-treatment step in the production of bio diesel from renewable feed stocks (Xu *et al.*, 2008).

Tantalum and Niobium pentoxides are also used themselves as photocatalysts for different processes such as: cleavage and purification of water (Stodolny & Laniecki, 2009; Prado *et al.*, 2008; Nakajima *et al.*, 2005), oxidation of organic contaminants (Esteves *et al.*, 2008), oxidation of alkanes (Ushikubo, 2000), partial oxidation of thiols to produce valuable synthons in pharmaceutical and agro chemistry (Budoace *et al.*, 2004), for esterification of β–keto esters (Sairre *et al.*, 2006) etc.

Due to close values of atomic and ionic radii of Niobium and Tantalum (Shannon, 1976) there is a possibility to obtain mixed oxides of general formula $(Nb_{1-x}Ta_x)_2O_5$, which are mainly used as photocatalysts for water decomposition (Kondo *et al.*, 2002; Zou *et al.*, 2002), catalysis (Yue & Gao, 2000), biomaterials, nanoporous materials for different applications and materials for optoelectronics (Yang *et al.*, 1998).

Niobium and Tantalum alkoxide complexes of common formula $M_2(OR)_{10}$ (M = Nb, Ta; R = Me, Et) are used as catalysts for the carboxylation of alcohols (Dibenedetto *et al.*, 2006) and deperoxidation of cyclohexyl hydro peroxide (Saint-Arroman *et al.*, 2008).

A special attention has been recently directed towards oxide nanobeads involving one or several early transition elements as perspective materials for Li-battery electrodes and for oxidation or acidic catalysis (Baruwati & Varma, 2010; Lee *et al.*, 2002). The structure-directing tools applied have in this case been either application of sol-gel technology in complex solvent mixtures (Baruwati & Varma, 2010) or using external templates (Lee *et al.*, 2002). Formation of spherical particles on uncontrolled hydrolysis of zirconium alkoxide precursors on liquid–air interface in contact with moist air has been reported, but the control of particle size and aggregation have not been achieved (Lin & Wang, 1988).

2 Problem definition

There are two important steps in the preparation of functional materials: the first one is synthesis of precursors and the second one the preparation of materials from them.

2.1 Rhenium

Among the Rhenium based catalysts the three most important ones are Rhenium metal, Rhenium oxides such as ReO_3, Re_2O_7 and of course MTO (methyltrioxorhenium, CH_3ReO_3). The preparation processes for these catalysts normally proceed under high temperatures and pressures (Okal, 2005; Räty & Pakkanem, 2000), sometimes starting with harmful substances like $(CH_3)_4Sn$ to obtain MTO (Jain & Kühn, 2007; Herrmann *et al.*, 1992).

The biggest limitation of Rhenium (VI) oxide catalyst is that ReO_3 can easily be reduced to inactive ReO_2 and all attempts to oxidize it to regenerate ReO_3 result in the loss of volatile Re_2O_7. Hence it is necessary to create conditions, permitting continuous functioning of these catalysts. It has been shown earlier that incorporation of ReO_3 into the NaY zeolite matrix can produce nanocomposites, where this oxide is more stable to the reducing conditions (Kustov *et al.*, 2004b; Kustov *et al.*, 2004a). The starting material for this catalyst was the oxomethoxide complex $Re_2O_3(OMe)_6$, which was obtained in one step by electrochemical synthesis (Kustov *et al.*, 2004b; Kustov *et al.*, 2004a; Seisenbaeva *et al.*, 2001). Both Re and Re_2O_7 based catalysts are usually obtained starting from ammonium or silver perrhenate (Naor *et al.*, 2010; Oikawa *et al.*, 2004; Wang *et al.*, 2003; Mandelli *et al.*, 2001; Doledec & Commereuc, 2000).

Normally, the preparation of rhenium oxide catalysts supported on TiO_2 from perrhenic acid involves such steps as impregnation of ReO_x centers

under inert atmosphere with subsequent calcination in the absence of oxygen (Secordel *et al.*, 2010).

2.2 Niobium and Tantalum

Unique properties of catalysts based on pentoxides of Ta and Nb, led recently to increased interest to mixed oxides based on both these metals. Several approaches to obtain mixed oxides are described in the literature. The common preparation method for the multicomponent oxides is usually via conventional solid-state reactions between binary oxides. This method was successfully implemented for the preparation of $(Nb_{1-x}Ta_x)_2O_5$ (Mohanty *et al.*, 1964), $Bi_3Fe_{0.5}Nb_{1.5}O_9$, (Lufaso *et al.*, 2007) and many other refractory materials. Unfortunately, the ceramic method requires heat treatment at rather high temperatures and leads to poorly homogeneous materials consisting of larger particles (Camargo & Kakihana, 2002). A number of alternative methods for preparation of multicomponent Nb or Ta oxides have been described. For instance, mixed oxides $SrNb_2O_6$ and $SrTa_2O_6$ were obtained via thoroughly mixing Nb or Ta hydroxides and commercially purchased Strontium hydroxide and prolonged heating at a relatively low temperature (400°C). The main limitation of this process is that it is multistep and applies the hydrofluoric acid in the preparation of the initial Nb and Ta hydroxides (Muthurajan *et al.*, 2008). Other alternative routes such as sol–gel synthesis based on metal-organic precursors, and the citrate method are often considered. Even the citrate method has such limitations as being a multistep and time-consuming procedure (Truijen *et al.*, 2007). For instance, $(Nb_{1-x}Ta_x)_2O_5$ solid solutions have been obtained by a neutral templating sol–gel method, using metal pentachlorides as precursors and a block copolymer as a template. According to this method, it is possible to obtain mesoporous $(NbTa)_2O_5$ oxide, which, however, contains chloride impurities (Katou *et al.*, 2002; Lee *et al.*, 2002). The mesoporous mixed oxides based on Nb and Ta or Mo can also be obtained by thermal decomposition of organic–inorganic precursors with the required ratio of metals in the molecular structure. The syntheses of precursors are complicated and involved several steps, hence providing relatively low yields of the final products (Deligne *et al.*, 2007; Bayot *et al.*, 2005). Moreover, the mesoporous Ta_2O_5 could be obtained by sol-gel process through several steps (Guo & Huang, 2011), using tantalum ethoxide $Ta(OEt)_5$.

Recently, in the literature was described a method for preparation of nanospheres based on Ta oxide. In this procedure tantalum butoxide was

added and subsequently hydrolyzed by adding the mixture of acetone and water (Baruwati & Varma, 2010).

Bi– and trimetallic alkoxide complexes can also be used, as precursors of complex oxides that contain required metals at the given ratios. Trimetallic complexes based on Rhenium, Niobium and Tantalum of the following formula $(Nb_{0.5}Ta_{0.5})_4O_2(OMe)_{14}(ReO_4)_2$ and $(Nb_{0.5}Ta_{0.5})_2(OMe)_8(ReO_4)_2$ with the Nb:Ta ratio 1:1 have been described earlier in (Shcheglov et $al.$, 2002). The synthesis of these complexes was based on the interaction between Re_2O_7 and a bimetallic alkoxide of Niobium and Tantalum, $NbTa(OMe)_{10}$ (Hubert-Pfalzgraf & Riess, 1975) (see $Fig.$ 2). It is possible to obtain these compounds due to isomorphous substitution for niobium atoms with tantalum ones, because the ionic radii of Nb and Ta for coordination number 6 are almost the same, 0.64Å (Shannon, 1976).

Thus, Re, Nb and Ta based materials are useful in almost all spheres of our life. Therefore, the starting point of this research was to develop further the approaches for preparation of precursors based on Re, Nb and Ta, investigate the properties of these complexes and compare them with already known compounds. The final aim was to obtain new functional materials based on these metals via controlled thermal decomposition and hydrolysis of the precursors.
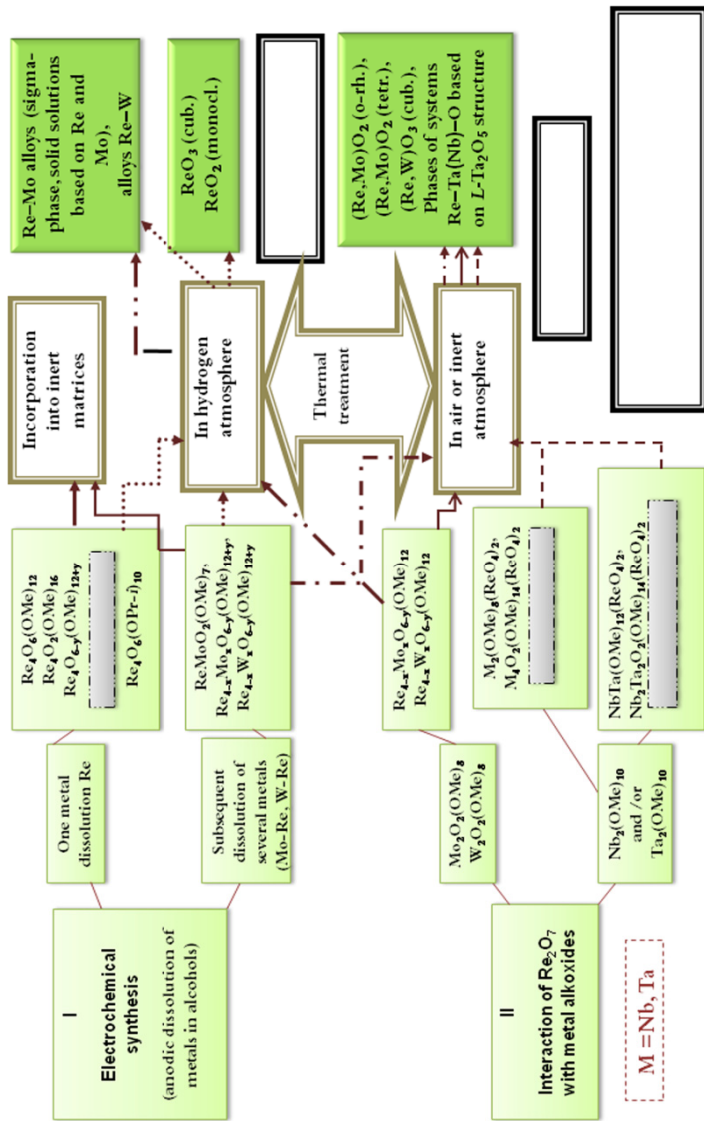
Figure 2. Scheme of preparation of the precursors and related materials

3 Objectives

The general aim of this work was to develop new molecular precursors and approaches to nanostructural multifunctional materials based on Re, Nb and Ta. We intended also to show the applicability of obtained materials. In order to achieve this goal, specific objectivities were formulated as follows:

➢ To synthesize new mono-, bi- and trimetallic complexes by already known methods.

➢ To investigate the effect of the ligand and metal ion ratio on the formation conditions and the chemical composition of the products of thermal treatment.

➢ To obtain different nanomaterials via thermal treatment of the precursors in different atmospheres.

➢ To prepare the catalysts from synthesized precursors and to test them in the catalytic oxidation reaction.

➢ To investigate the hydrolysis of all synthesized complexes and to optimize the formation of nanostructural materials (nanobeads).

4 Experimental

Two major approaches to obtain mono-, bi- and trimetallic complexes on the basis of rhenium, niobium and tantalum used in this work were (1) the electrochemical method (for the synthesis of monometallic complexes) and (2) the interaction of rhenium heptoxide with alkoxo-derivates of niobium and/or tantalum. The main advantage of anodic dissolution is a high productivity and simplicity in comparison with the traditional methods based on substitution reactions. The interaction of Re_2O_7 with $M_2(OR)_{10}$ where $M = Nb$, Ta and $R = Me$, Et allows to obtain not only the bimetallic but also the trimetallic complexes of the common formula $(M_{1-x}M'_x)_4O_2(OR)_{14}(ReO_4)_2$ ($M = Nb; M' = Ta; R = Me, Et, {}^nPr$), where x = 0–1 in a single step, the main advantage of this method.

The thermal decomposition of monometallic ethoxocomplex leads to formation of nanoparticles of metallic Re, in the case of trimetallic methoxocomplexes – formation solid solutions mixed oxides which are related to the block structures of the H-modification Nb_2O_5 and the L-modification Ta_2O_5. Thermal decomposition in air of these complexes leads to formation porous mixed oxides, with the structures related to the block structure of the L-modification of Ta_2O_5.

Deposition of mono- and bimetallic complex $Re_4O_4(OEt)_{12}$ **(I)** and $Ta_4O_2(OEt)_{14}(ReO_4)_2$ **(III)** on TiO_2 (anatase form) support with subsequent thermal treatment leads to formation of two type of catalysts ReO_x/TiO_2 and $ReO_x/Ta_2O_5/TiO_2$ respectively.

The Sol-Gel technique was successfully applied in order to obtain the nanostructural materials (nanobeads) from bi- and trimetallic complexes.

4.1 Synthesis of precursors

Handling of the complexes and all procedures connected with synthesis were carried out in inert (nitrogen) atmosphere in a dry box. Methanol was purified by distillation over magnesium methoxide. Dry ethanol (less than 0.02% H_2O, cat № 100990) was purchased from MERCK and used without further purification. Hexane and toluene were purchased from Aldrich and dehydrated by refluxing over $LiAlH_4$ with subsequent distillation. LiCl for electrochemical experiments has been dried in air at $120 - 150$ °C for at least 4 h and then in dynamic vacuum (P~1.3 Pa) at $180 - 200$ °C for 1 h. Rhenium heptoxide was purchased from Aldrich with purity 99.9+%. The $Ta(OCH_2CH_3)_5$ 99+% (L10288) and $Nb(O^nC_3H_7)_5$ 99% (36571) were purchased from Alfa Aesar.

The alkoxides, $Nb_2(OR)_{10}$ and $Ta_2(OR)_{10}$ (R = Me, Et), used in this work as starting materials for the synthesis of bi- and trimetallic complexes, were prepared by anodic oxidation of the corresponding metals in methanol or ethanol respectively and purified according to conventional techniques (Turova *et al.*, 1996; Turevskaya *et al.*, 1995).

$Re_4O_4(OEt)_{12}$ (I) Rhenium was dissolved in ethanol in the electrochemical cell without subdivision into cathode and anode space, supplied with a reflux condenser and water-cooling. LiCl was added as electrolyte. The electrolysis was associated with color changes from colorless to yellow and finally to reddish brown. Crystallization of dark brown plates was observed already during the process of electrochemical synthesis. The crystals were separated by decantation at the end of the process.

$Nb_4O_2(OEt)_{14}(ReO_4)_2$ (II) $Nb_2(OEt)_{10}$ was dissolved in dry toluene. Re_2O_7 was added to the obtained solution and was stirred until complete dissolution. The mixture was quickly heated to 60 °C and cooled to the room temperature (r.t.). Then, one sample (**II**) was left for 24 h for crystallization at r.t. (22 °C), and the second one (**IIa**) was put into a freezer (-15 °C). Yellow crystals have appeared. The solvent was removed by decantation and the crystals were dried *in vacuum* at r.t.

$Ta_4O_2(OEt)_{14}(ReO_4)_2$ (III) A procedure analogous to that for compound **II** was applied, using $Ta_2(OEt)_{10}$ and Re_2O_7. Two samples were crystallized at the two different temperatures: one (**III**) at 22 °C and other one (**IIIa**) at (-15 °C). Then, the mother liquor was removed by decantation and the practically colorless crystals were dried *in vacuum* at r.t.

Nb₄O₂(OMe)₁₄(ReO₄)₂ (IV) and Ta₄O₂(OMe)₁₄(ReO₄)₂ (V) Complexes were obtained as described in (Seisenbaeva & Kessler, 2001; Seisenbaeva *et al.*, 2001) compare with the complexes (**II**) and (**III**).

(Nb₀,₇Ta₀,₃)₄O₂(OMe)₁₄(ReO₄)₂ (VI) $Nb_2(OMe)_{10}$ and $Ta_2(OMe)_{10}$ were dissolved in 3.5 and 2.5 ml of toluene respectively and then solutions were poured together and mixed in order to achieve Nb:Ta = 0.7:0.3 ratio. Rhenium (VII) heptoxide was added to the obtained solution upon stirring. During dissolution of Re_2O_7 the color of solution changed from light green to pinkish-brown. At the end of the process the mixture was heated to 50 °C and the color of the solution became dark brown with red nuance. Then mixture was refluxed during 3–5 min and then cooled to r.t. and left for crystallization. After 24 hours the solution was decanted and the crystalline product (thick needle shaped crystals light lilac in color) was dried *in vacuum* at r.t.

(Nb₀,₃Ta₀,₇)₄O₂(OMe)₁₄(ReO₄)₂ (VII) In order to obtain this complex the same procedure as described above for complex (**VI**) was applied.

(Nb₀,₅Ta₀,₅)₄O₂(OMe)₁₄(ReO₄)₂ (VIII) $(Nb_{0,5}Ta_{0,5})_4O_2(OMe)_{14}(ReO_4)_2$ complex was obtained as described in reference (Shcheglov *et al.*, 2002) to compare with the complexes (**VI**) and (**VII**).

(NbₓTa₁₋ₓ)₄O₂(OEt)₁₄(ReO₄)₂ (IX) is analogous to $(Nb_xTa_{1-x})_4O_2(OMe)_{14}(ReO_4)_2$ (**VIII**) complex which was obtained as described in (Shcheglov *et al.*, 2002). To obtain complex **(IX)** Niobium ethoxide $Nb_2(OEt)_{10}$ (0.279 g, 0.440 mmol) and Tantalum ethoxide $Ta_2(OEt)_{10}$ (0.356 g, 0.440 mmol) were dissolved in 2.5 ml and 3.5 ml of toluene, respectively, and then solutions were mixed to achieve the Nb:Ta = 0.5:0.5 ratio. Rhenium heptoxide (VII) Re_2O_7 (0.212 g, 0.438 mmol) was added to the obtained solution upon stirring and stirred further in 30 min at 25 – 30 °C until Re_2O_7 was dissolved completely. During dissolution of Re_2O_7, the color of solution changed from light yellow to light brown. At the end of the process, the mixture was heated to 50 °C and the color of the solution became brown. Then solution was cooled to r.t. and left for crystallization. After 24 h, the mother liquor was decanted and the crystalline product (thick needle-shaped colorless crystals) was dried in vacuum.

Nb$_4$O$_2$(O^{n}Pr)$_{14}$(ReO$_4$)$_2$ (X) complex has been obtained in the same way as its analogs, **Nb$_4$O$_2$(OEt)$_{14}$(ReO$_4$)$_2$ (II)**, **Nb$_4$O$_2$(OMe)$_{14}$(ReO$_4$)$_2$ (IV)**, **Ta$_4$O$_2$(OEt)$_{14}$(ReO$_4$)$_2$ (III)** and **Ta$_4$O$_2$(OMe)$_{14}$(ReO$_4$)$_2$ (V)**. The Nb$_2$(O^{n}Pr)$_{10}$ (0.325 g, 0.419 mmol) was dissolved in 5 ml of toluene and then Rhenium heptoxide, Re$_2$O$_7$ (0.127 g, 0.262 mmol) was added to the obtained mixture. All other procedures were the same as described above.

4.1.1 X-ray crystallography

For the X-ray single crystal studies the data collection was carried out at r.t. using a Bruker SMART CCD 1 K diffractometer at the Department of Chemistry, SLU and at T = 100 K using an Excalibur with sapphire-3 CCD detector (Oxford Diffraction Ltd.) at the Department of Materials and Environmental Chemistry, Stockholm University (MoKα radiation, graphite-monochromator) for the experimental details see Table 1. The structures were solved by direct methods. Metal atom coordinates were located in the initial solution and all the other non-hydrogen atoms in the subsequent difference Fourier synthesis. All non-hydrogen atoms were refined by full matrix techniques, first in isotropic and then in anisotropic approximation. The coordinates of the hydrogen atoms were calculated geometrically and introduced in the final refinement in isotropic approximation using a riding model. All calculations were performed using SHELXTL-NT program package (SHELXTL-NT, 1998) and Apex II on a on a personal computer. Empirical adsorption correction was made applying the SADABS program.

Table 1. *Crystal data and diffraction experiments*

Complex	I	II	IIIa	III	IV	V	IX	X
Space group	P –1		P2$_1$/n		P2$_1$/c		P2$_1$/n	
Crystal system	Triclinic	Monoclinic						
a, Å	8.359(7)	13.175(5)	12.774(1)	13.227(5)	9.854(6)	10.002(2)	13.165(5)	14.063(6)
b, Å	10.482(1)	13.532(2)	13.224(9)	13.453(6)	16.001(1)	13.451(4)	13.484(6)	14.446(6)
c, Å	11.809(2)	14.951(5)	14.855(1)	14.982(7)	12.331(8)	14.233(3)	14.961(7)	17.076(8)
β, °	72.282(1)	99.967(2)	100.58(8)	100.408(1)	100.860(1)	109.763(6)	100.422(1)	100.115(9)
V, Å^3	938	2625(1)	2470.9(4)	2622(2)	1908(2)	1802.2(8)	2612.2(2)	3415(3)
T, K	153	295	100	295	295	295	295	296
Number of independent reflections	7090	2808	6864	2806	2179	5374	5231	5156
(R$_{int}$)	(0.0492)	(0.0480)	(0.0827)	(0.1303)	(0.0706)	(0.0540)	(0.0975)	(0.0851)
R$_1$	0.0377	0.1091	0.0970	0.1239	0.0868	0.0493	0.0771	0.0928
wR$_2$	0.0792	0.1968	0.1807	0.1513	0.1197	0.1001	0.1771	0.2315
GoF<F^2>	0.921	1.083	0.990	0.921	0.974	0.925	1.081	1.174

4.2 Preparation of nanostructural materials

4.2.1 Metal-organic decomposition

The thermal decomposition of complex (**I**) was carried out with a Perkin-Elmer TGA-7 device in nitrogen atmosphere in the temperature range 20–450 °C with a heating rate 10 °C/min.

The thermal treatment of trimetallic methoxide complexes (**VI**), (**VII**) and (**VIII**) were performed in the Q–1500 D instrument at the temperature 1000 °C with a heating rate 5 °C/min in air, and in a Perkin-Elmer TGA-7 device at 900 °C with a rate 10 °C/min in nitrogen atmosphere.

4.2.2 Sol-Gel

Two types of hydrolysis: natural and accelerated have been applied to obtain spherical aggregates denoted below as nanobeads. Certain masses of the precursor crystals were taken from the mother liquor and dissolved in different volumes of toluene, depending on the solubility of the alkoxides. Natural hydrolysis was carried out by slow diffusion of the ambient atmosphere into a flask with solution of alkoxide precursor connected with air through a syringe needle piercing the serum cup. The accelerated hydrolysis was carried out by addition of liquid water in two different protocols: (1) 0.01 ml of H_2O was quickly added by syringe on shaking to 0.5 ml of toluene solution of the precursor, or (2) 0.05 ml of the respective alcohol (depending from precursor) and 0.01 ml of H_2O were added consequently by syringe on shaking to 0.5 ml of toluene solution of the precursor. Directly after addition of water milky colloid solution was obtained with following formation of nanobeads in both cases. The particles were separated by centrifugation with subsequent removal of solvent by decantation and dried in vacuum.

Starting solutions for preparation of nanobead samples were obtained by dissolution of 1.017 g of (**IX**) in 7 ml toluene, for the synthesis of **NBI**, **NBI⋆** and **NBI⋆⋆** respectively (the first sample originating from natural hydrolysis, the one marked with one star – from accelerated hydrolysis with pure water and the one with two stars – from accelerated hydrolysis by water in parent alcohol); 0.121 g of (**X**) in 3 ml toluene were used for **NBIII**, **NBIII⋆** and **NBIII⋆⋆**; 0.294 g of (**II**) in 4.8 ml toluene were used for **NBIV**, **NBIV⋆** and **NBIV⋆⋆**; and 0.719 g of (**III**) in 2 ml toluene were used for the synthesis of **NBVI** and **NBVI⋆**. Poor solubility of precursors

28

(**VIII**) and (**IV**) hinder preparation of the corresponding nanobead materials from them (numbering of nanobead samples is the same as in the paper VI).

4.2.3 Solution deposition

Support The TiO_2-anatase support (Titanium (IV) oxide catalyst support, Alfa Aesar) was calcined before use at 250 °C overnight in air and then transferred to a dessicator to avoid any traces of humidity.

Catalysts preparation was carried out in two steps: the former involving impregnation of the TiO_2-support with a calculated amount of alkoxide solutions and the latter with thermal treatment of the catalysts at 300 °C in air for 2 h with an initial heating rate of 5°C/min. In both steps we had, as we expected, some losses of the Re presumably as Re_2O_7, due to the volatility of this oxide, and also of the organic part of the alkoxide complexes.

To obtain 1 wt% (**S1**) and 2 wt% (**S2**) of ReO_3/TiO_2 the calculated volumes of $Re_4O_4(OEt)_{12}$ alkoxide solution (0.032 mmol and 0.064 mmol) were used to impregnate 2.97 g and 2.94 g of pretreated TiO_2-support respectively, followed by stirring of the mixture until complete infusion of alkoxide solutions into TiO_2. The samples were then dried in vacuum and left overnight to dry in air at room temperature. The next step of preparation was calcination of catalysts at 300 °C in air for 2 h with an initial heating rate 5 °C/min. The mass losses were not significant and observed for **S1** and **S2** as 2 wt%.

The desired amount of $Ta_4O_2(OEt)_{14}(ReO_4)_2$ alkoxide solution (0.064 mmol and 0.641 mmol) was used accordingly to prepare 1 wt% (**S3**) and 10 wt% (**S4**) of $ReO_3/Ta_2O_5/TiO_2$ catalysts. The applied procedures of impregnation with alkoxide solutions (**III**) were the same as described above. After thermal treatment of catalysts the weight losses were observed as 5 wt% for both samples.

To provide an experimental reference to the catalytic activity of **S3** and **S4** catalysts, a material with 7 wt% TaO_x/TiO_2 (**S5**) was synthesized using $Ta_2(OEt)_{10}$ as starting material. The aforementioned techniques were used for the preparation of this catalyst (**S5**). The calculated amount of $Ta_2(OEt)_{10}$ 1.9 mmol was impregnated on 4.65 g of pretreated TiO_2. After the thermal treatment the weight loss was about 4 wt%, which corresponds only to release of the organic part of the precursor.

4.3 Characterization of precursors and materials

Several techniques were used for characterization of the obtained complexes and their derivatives.

The infrared (IR) spectra of Nujol, hexachlorobutadiene mulls and solid state FT-IR measurements in KBr pellets were recorded with a Perkin Elmer FT-IR spectrometer Spectrum-100. To establish the exact peak positions the fitting of the peaks was carried out using Origin software.

Mass-spectra were recorded using JEOL JMS-SX/SX–102A mass-spectrometer applying electron beam ionization (U = 70 eV) with direct probe introduction. The decomposition and sublimation processes in vacuum were studied in glass vessels evacuated by oil pump (p = 10^{-2} mm m.c.). The gaseous products of decomposition were collected in the Schlenk traps cooled with liquid nitrogen. After the decomposition process was accomplished, the system was filled with dry nitrogen and after warming to r.t. a sample of the gas phase from the trap was investigated by GC-MS using Hewlett Packard 5890 Series II gas chromatograph supplied with capillary separating column connected to JEOL JMS-SX/SX102A mass spectrometer.

The results of microanalysis (C, H) were performed by Mikrokemi AB, Uppsala for (**I**) and for complexes (**II – VIII**) on a Heraeus CHN-O-RAPID instrument (standard deviations: C±0.3%, H±0.1%) at the laboratory of Organic Analysis of the Moscow State Academy of Fine Chemical Tehnology.

^{1}H and ^{13}C NMR spectra were registered for $CHCl_3$ solutions on a Bruker DRX 400 MHz instrument at 300 K.

Thermal analysis (DTA-TGA) was carried out in air at a heating rate 5 °C/min, using Q–1500 D (F. Paulik, J. Paulik, L. Erdey) instrument using 120-300 mg samples (weighing accuracy, ±0.4 mg) at the Department of Chemistry and Technology of Rare Elements of the Moscow State Academy of Fine Chemical Technology. Thermo-gravimetric (TG) studies were carried out with a Perkin-Elmer TGA-7 or Pyris 1 device and the measurements were performed in nitrogen atmosphere, with the samples of 10–15 mg. The DSC thermograms were recorded with a Perkin-Elmer DSC-2 apparatus at the Department of Materials and Environmental Chemistry of the Stockholm University. The DSC equipment was calibrated both on temperature scale and enthalpy by use of metallic Tin.

X-ray powder diffraction (XPD) studies were carried out on a DRON-3M powder diffractometer (CuKα radiation, scan step of 0.05°-0.1°, counting time of 2-4 s per data point) at the Department of Chemistry and Technology of Rare Elements of the Moscow State Academy of Fine

Chemical Technology and by Guinier-Hägg method using CuKα radiation and silicon as internal standard and with a STADI-P (STOE) diffractometer at the Department of Materials and Environmental Chemistry, Stockholm University. The powder patterns were obtained by scanning of the original films using the SCANPI program (Johansson et al., 1980; Malmros & Werner, 1973). The X-ray powder data collection was also carried out at room temperature using a Bruker APEX II diffractometer (MoKα radiation, graphite-monochromator) at Department of Chemistry, SLU.

Theoretical analysis of bonding in $Re_4O_4(OEt)_{12}$ was carried out on the basis of molecular orbital diagrams calculated using extended Hückel theory (EHT) level with the use of the CACAO (Mealli & Proserpio, 1990) program package, applying a model with CH_3-groups as simplified analogs of Et and ^iPr-ones for orbital diagram calculations were made by A.I. Baranov and A. V. Shevelkov.

EXAFS – Data collection. Tantalum and Rhenium Kα edge X-ray absorption spectra were recorded at the wiggler beam line I811 at the MAXLab, Lund University, Lund; Sweden. The EXAFS station was equipped with a Si [111] double crystal monochromator. The data collection was performed in transmission mode. Higher order harmonics were reduced by detuning the second monochromator to 30 % of maximum intensity at the end of the scans. The energy scale of the X-ray absorption spectra were calibrated by assigning the first inflection point of the K edge of a tantalum foil to 9881 eV (Thompson *et al.*, 2001). The EXAFSPAK program package (George & Pickering, 1993) was used for the data treatment.

SEM micrographs of the samples were obtained with a HITACHI TM-1000 scanning electron microscope equipped with an EDX detector. To obtain reliable statistics in the analysis the data for each point were taken as average of 10 single measurements. The mapping across the analyzed surface was made by moving over the sample with steps of 8 μm.

Transmission electron micrographs and electron diffraction (ED) patterns of the samples in a JEOL 2000FX-II transmission electron microscope (TEM), equipped with a Link AN-10000 energy dispersive spectrometer (EDS) for microanalysis studies and HRTEM investigations on a JEOL JEM-2100F transmission electron microscope were obtained at the Department of Materials and Environmental Chemistry, Stockholm University.

Catalytic activity measurements were made using a fixed bed reactor described elsewhere (Royer *et al.*, 2007). Two different conditions in terms of methanol concentration were studied applying 7% methanol (poor

condition) and 40% methanol (rich condition) diluted by air. After having passed through the catalytic bed, the reaction products were analyzed by on-line μ–gas chromatography (SRA) equipped with Poraplot U and 5Å molecular sieve columns and TCD detectors. All the lines carrying methanol or reaction products were warmed up to 80 °C by heating tapes (Horst) to avoid condensation.

The specific surface areas of the catalysts were measured on a Quanta chrom – Quanta sorb apparatus using the single point BET method.

The XPS analyses were performed using a Kratos Analytical AXIS UltraDLD spectrometer. A monochromated aluminium source (AlKα = 1486.6 eV) was used for excitation. The X-ray beam diameter was approximately 1mm. The analyser was operated at constant pass energy of 40 eV using an analysis area of approximately 700 μm x 300 μm. Charge compensation was applied to compensate for the charging effects that occurred during the analysis. The C 1s (285.0 eV) binding energy (BE) was used as internal reference. The spectrometer BE scale was initially calibrated against the Ag $3d_{5/2}$ (368.2 eV) level. Pressure was in the 10-10 torr range during the experiments. Simulation of the experimental photo peaks was carried out using CasaXPS software. Quantification took into account the non–linear Shirley (Shirley, 1972) background subtraction. The decomposition of the doublet Re $4f_{7/2}$ – Re $4f_{5/2}$ was performed considering the spin–orbit splitting of 2.4 eV.

5 Results and Discussion

5.1 Precursors

5.1.1 Synthesis and structure of precursors

The anodic dissolution of Re in ethanol **(Paper I)** leads to formation a complex following formula $Re_4O_4(OEt)_{12}$ **(I)** which contains planar Re_4– core close to a rhombus in its geometry (*see Fig. 3*). It was shown earlier that this process is a productive approach to the alkoxide derivates of Rhenium and it was investigated in such solvents as methanol and isopropanol (Seisenbaeva *et al.*, 2004; Seisenbaeva *et al.*, 2001; Shcheglov *et al.*, 2001; Kessler *et al.*, 1995). The anodic dissolution of Rhenium in these solvents leads to formation of tetranuclear oxoalkoxide compounds, $Re_4O_{6-x}(OMe)_{12+x}$, containing mainly Re(VI) (Seisenbaeva *et al.*, 2001; Kessler *et al.*, 1995) and of $Re_4O_6(O^iPr)_{10}$ (*see Fig. 3*), were two atoms of Re(V) and two of Re(VI) were present in the same molecule (Seisenbaeva *et al.*, 2004; Seisenbaeva *et al.*, 2001; Shcheglov *et al.*, 2001).

The structure of (**I**) belongs as well as the structure of the oxo isopropoxide $Re_4O_6(O^iPr)_{10}$ to the well known M_4X_{16} core type structure. These structures have a hexagonal dense packing of metal atoms and ligands, one of the most typical for metal alkoxides (Turova *et al.*, 2002; Wright & Williams, 1968). It should be mentioned, that for such structures the $M-M$ bonds are typically present. There are several compounds where for such bonding different number of cluster electrons is available. For example, in the structure of compound (**I**) 8 electrons are available for 5 M–M bonds. Two symmetrically equivalent long bonds of 2.63 Å, two other symmetrically equivalent short bonds 2.5358(5) Å and the shorter diagonal of the rhombus, which has almost the same lengths 2.5511(5) Å, have been observed.
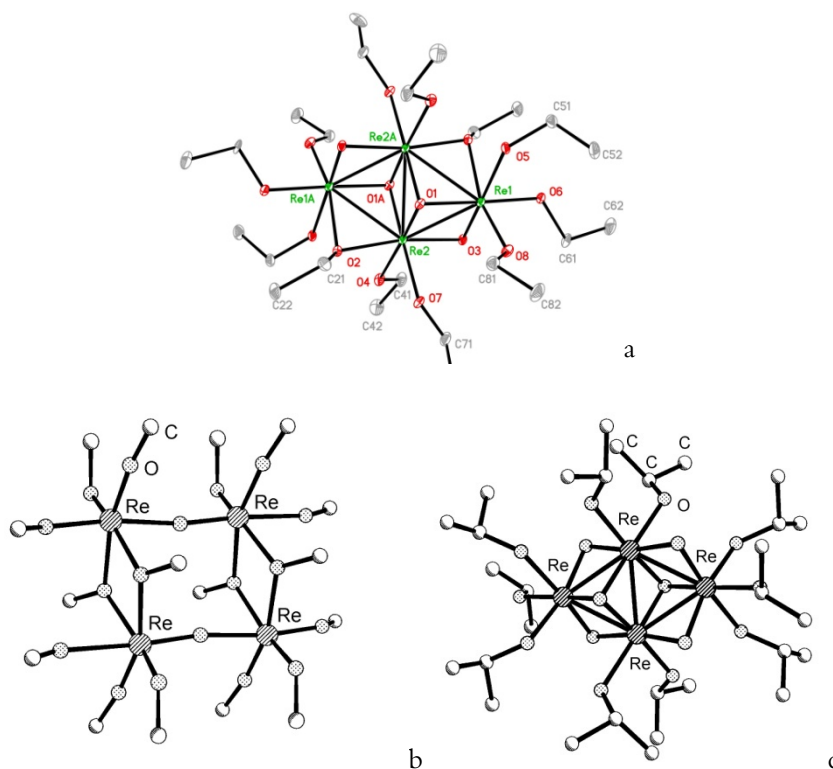
Figure 3. Molecular structures of Rhenium alkoxide homolog's: a − $Re_4O_2(OMe)_{16}$, b − $Re_4O_4(OEt)_{12}$, c − $Re_4O_6(O^iPr)_{10}$

The same bond arrangement was found also in the structure of $W_4(OEt)_{16}$ (Chisholm *et al*., 1981), where the longer side of the rhombus was found to be 2.94 Å, the shorter side being 2.65 Å and the short diagonal − 2.76 Å. In the Rhenium isopropoxide for the same 5 M–M bonds only 6 cluster electrons are available and the bond lengths are almost the same 2.52 − 2.55 Å (Seisenbaeva *et al*., 2004; Shcheglov *et al*., 2001). The known 4-electron systems reveal only two localized M –M bonds, as it has been observed in $Mo_4O_8(O^iPr)_4Py_4$ (Chisholm *et al*., 1984).

The *Fig. 3* provides comparison between the structures of all three monometallic compounds. For the methoxide Re(VI)-compound the structure contains only 2 oxo-bridges as each metal center can contain 4 alkoxide ligands in its surrounding, the ethoxocomplex involves already 4 oxo-bridges to compensate the possibility of putting together 2 metals atoms connected with 4 alkoxide ligands and 2 − with only 3 such ligands. The isopropoxide ligand size is already too big and the structure, following the

same dense packing as for the $Re_4O_4(OEt)_{12}$, hosts 2 metal atoms with 3 alkoxide ligands and 2 – with only 2 alkoxide ones.

The bimetallic complexes (**II**), (**III**) and (**X**) (**Paper II** and **VI**, respectively) have been prepared via interaction of Rhenium heptoxide, Re_2O_7, and Niobium and Tantalum alkoxides, $M^v_2(OR)_{10}$ (R = Me, Et, ^nPr), in hydrocarbons. Samples were crystallized at room temperature 22 °C and at low temperature -15 °C for all compounds. The structures of these compounds were determined by X-ray single crystal diffraction (see *Table 1*). Their molecular structures (see *Fig. 4*) are based on a tetranuclear $M_4(\mu$-$O)_2(\mu$-$OR)_4X_{12}$ core, X = OR, ReO_4, with rectangular planar M_4-arrangement (M = Nb, Ta), composed of two pairs of edge-sharing octahedra, joined via two almost linear oxo-bridges. The perrhenate ligands are attached in a centrosymmetric manner to the two opposite corners of the rectangle (see *Fig. 4*). Only, for complex **III** two different modifications were discovered at room temperature (sample **III**) and at low temperature (**IIIa**) (see Table 1 in Paper II).
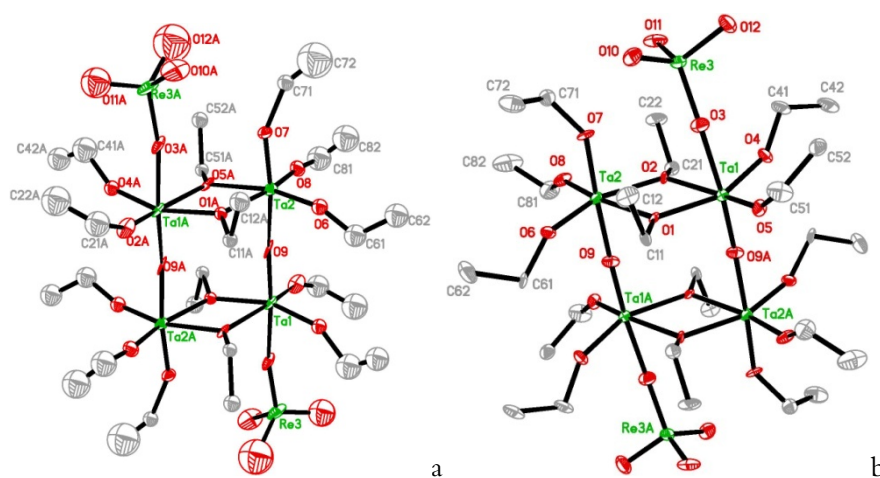

Figure 4. Molecular structures of the **III** and **IIIa** samples of $Ta_4O_2(OEt)_{14}(ReO_4)_2$: a – sample crystallized at 22 °C; b – sample crystallized at – 15 °C.

Two different modifications of $Ta_4O_2(OEt)_{14}(ReO_4)_2$, which were crystallized at the different temperatures, differ considerably in the values of unit cells parameters and density of the samples. For the sample **IIIa** the density is much higher than for the sample **III**, which is connected with temperature of crystallization. It is to be noted that in case of methoxo complexes the decrease in crystallization temperature led to formation of new non-oxo methoxocomplexes of the common formula

$M_2(OMe)_8(ReO_4)_2$, where M = Nb, Ta (Shcheglov *et al.*, 2002; Seisenbaeva & Kessler, 2001). This difference between methoxides and ethoxides, and npropoxide is caused evidently by easier oxidation of ethanol and propanol resulting in release of water and formation of oxo-species. Thus, we can conclude that the temperature of crystallization influences mostly the unit cell parameters; density and volume of the unit cell, but not so much the chemical nature of the products and the bond lengths (*see Table 1*).

The temperature of crystallization affects also substantially the perrhenate group geometry. For the samples **II**, **III**, **IV** and **V** it was observed that the perrhenate group had ideal tetrahedral geometry (see Table 2 in Paper III) in contrast to sample **IIIa** (crystallized at low temperature), where the same group was distorted due to interaction with an ethoxo-group in the packing. The size of alkoxide ligand is influencing the position of the perrhenate group. Comparing the ReM1M2 and ReM1M(2A) angles (see *Fig. 3* and Table 3 in Paper III) for all complexes it was found that in the methoxocomplexes **IV** and **V**, the ReO_4^- group is turned toward the terminal methoxo group due to the smaller volume of a free space in the crystal lattice of these complexes. For ethoxo complexes **II**, **III** and **IIIa** the perrhenate group is turned toward the bridging ethoxo group. It should be mentioned, that ReM1M(2A) angles decrease from the sample **II** to sample **V** and ReM1M2 angles increase in the same series, which is, obviously, connected with the increasing size of the alkoxide ligand. The same tendency we can observed comparing complex (**X**) with its ethoxides and methoxides analogs. The perrhenate group in (**X**) is turned toward the bridging propoxo group (see Paper VI).

The trimetallic oxoalkoxide complexes of the common formula $(Nb_xTa_{x-1})_4O_2(OR)_{14}(ReO_4)_2$, where x = 0.3, 0.5, 0.6, 0.7 and R = Me, Et (**Paper IV** and **VI**) can be obtained via interaction of $Nb_2(OR)_{10}$ and $Ta_2(OR)_{10}$ (R = Me, Et) with Re_2O_7 in toluene. Previously, it was observed that isomorphous replacement of Niobium by Tantalum atoms in the structure allows to obtain trimetallic complexes of following compositions $(Nb_{0.5}Ta_{0.5})_4O_2(OMe)_{14}(ReO_4)_2$ and $NbTa(OMe)_8(ReO_4)_2$ (Shcheglov *et al.*, 2002).
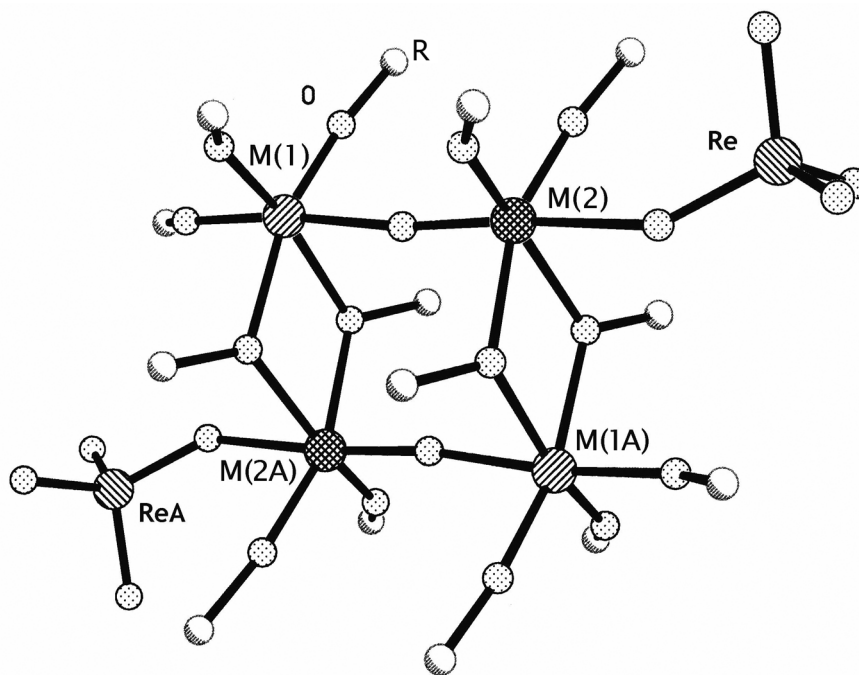
Figure 5. The molecular structure of trimetallic complexes of common formula $(Nb_xTa_{x-1})_4O_2(OR)_{14}(ReO_4)_2$, where x = 0.3, 0.5, 0.7, R = Me, Et.

In order to obtain new complexes $(Nb_{0.7}Ta_{0.3})_4O_2(OMe)_{14}(ReO_4)_2$ (**VI**), $(Nb_{0.3}Ta_{0.7})_4O_2(OMe)_{14}(ReO_4)_2$ (**VII**) and $(Nb_{0.6}Ta_{0.4})_4O_2(OEt)_{14}(ReO_4)_2$ (**IX**) the same method as for $(Nb_{0.5}Ta_{0.5})_4O_2(OMe)_{14}(ReO_4)_2$ complex (**VIII**) was applied. The molecular structures of (**VI**) and (**VII**) are analogous to the structures of (**II**), (**III**), (**IV**), (**V**), (**VIII**) and (**X**), and is shown in *Fig 5*. The results of solution and refinement of the structure show significant distinctions between the unit cell parameters of the samples (*see Table 1*). As it can be seen from the results, the unit cell parameters and related characteristics, i.e. density and volume of the unit cell, are depending on ratio between Niobium and Tantalum in the complexes. It was found earlier that the distribution of metals for the (**VIII**) complex in the crystallographic positions in the structure is uneven. The atoms of Niobium are mainly placed in the M1 "oxo"-position (see *Fig. 5*), i.e. the position in which the atom of metal is connected with a perrhenate ReO_4^- group through an oxo-bridge, and the atoms of tantalum are mainly situated in the M2 "alkoxo"-position. Occupation of the first position composes approximately 70% Nb + 30% Ta, while the latter one 30% Nb + 70% Ta

(Shcheglov *et al.*, 2002). This trend in distribution of metal atoms is preserved for the trimetallic oxoalkoxo complex with ratio between Nb and Ta 70:30 according to the structure refinement statistics. For the $(Nb_{0,3}Ta_{0,7})_4O_2(OMe)_{14}(ReO_4)_2$ complex this distribution is not traced evidently because of increased tantalum content in the compound. The same tendency can be seen in the ethoxocomplex (**IX**), but the distribution of niobium and tantalum atoms is even more preferential: in oxo–position M1 is situated 85% of niobium and 15% of tantalum atoms while in alkoxo–position M2 35% of Nb and 65% of Ta are present (see Paper VI). According to the structure refinement statistics the ratio between Nb and Ta in the $(Nb_xTa_{1-x})_4O_2(OEt)_{14}(ReO_4)_2$ complex is 60:40, while for the trimetallic methoxide complex (**VIII**) this ratio is 50:50.

It should thus be concluded that it is the increased niobium content (Nb:Ta = 1:1 and higher) that favors the uneven distribution of metals cations. The contents of Niobium and Tantalum in the composition of trimetallic complexes influences the parameters and the volume of unit cell, which vary with the increase in the tantalum content and decrease in the niobium content in the oxomethoxo complexes. The decrease in volume of the unit cell in the series from $(Nb_{0,7}Ta_{0,3})_4O_2(OMe)_{14}(ReO_4)_2$ to $(Nb_{0,3}Ta_{0,7})_4O_2(OMe)_{14}(ReO_4)_2$ is observed from the results of solution and refinement of the structures (see Table 01 in Paper IV), and connected with prevalence of the statistic distribution of metals in occupation of the crystallographic positions in the structure (**VI**). It should also be mentioned, that the increase in ligand size also influences the parameters and volumes of the unit cell in all trimetallic complexes (*see Table 1*).

5.1.2 Characterization of precursors

From the results of solution and refinement of the structures and IR spectroscopic investigation for all complexes it is confirmed that the size of ligands influences the bonds lengths.

The latter is evident from comparison of the IR spectra of complex (**I**) with the other rhenium alkoxides (see *Table 2*). The increase in the steric tension with incorporation of a bigger alkoxide ligand can even be traced in the increase in the terminal bond lengths on the change in the alkyl group: in the structure of $Re_4O_6(OMe)_{12}$ it is 1,883(7)-1,936(7)Å (Seisenbaeva *et al.*, 2001), in that of the ethoxide, $Re_4O_4(OEt)_{12}$ (**I**) −1,941(14)-2,13(2)Å, and in that of the isopropoxide, $Re_4O_6(O^iPr)_{10}$, − 1,950(5)-2,148(6)Å (Shcheglov *et al.*, 2001). The vibrations at 869–970 cm^{-1} can be related to the spectral region of asymmetric Re–O–Re stretching vibrations for all complexes, the bond lengths of which become shorter from $Re_4O_2(OMe)_{16}$

to $Re_4O_6(O^iPr)_{10}$ due to the increased size of the alkoxide ligand. The increasing donor properties of the alkyl radical do not lead thus to any shortening in the metal–oxygen bond lengths.

Table 2. *IR - spectra of Rhenium complexes*

Compound			Vibration
$Re_4O_2(OMe)_{16}$★	$Re_4O_4(OEt)_{12}$	$Re_4O_6(O^iPr)_{10}$★	
1166 m	1167 w	1165 m	
1123 m	1154 w	1140 m	
		1114 s	ν (C–O) + δ (C–H)
1069 m	1082 w		
1038 s			
1021 s	1005 w	1020 m	
966 s br	979 w	965 st	ν (Re=O)
	906 s	926 m	ν (Re–O–Re)
870 sh		840 m	ν (C–C)
		814 m	
783 w	769 sh	755 m	
		703 w	δ (C–H)
		614 m	ν (Re–OR_terminal)
597 m		592 m	
564 s		552 w	
544 m			ν (Re–OR_мост)
	461 m	475 w	ν (Re–OR_bridge, terminal) +δ (C–C)
431 m		452 w	
★ – literature (Seisenbaeva *et al.*, 2001; Shcheglov *et al.*, 2001)			

To characterize the bulk sample of the complex (**I**) the XPD analysis was performed and it revealed that (**I**) was not stable in ambient atmosphere. The X-ray powder pattern of $Re_4O_4(OEt)_{12}$, taken from the fresh sample **I,** indicates difference in peaks positions and intensities from the pattern which was generated by ATOMS software (ATOMS, 2006) based on the parameters from the single crystal X-ray study of (**I**). Therefore, a pattern of a hypothetical structure model $Re_4O_6(OEt)_{10}$ related to $Re_4O_6(O^iPr)_{10}$ (Seisenbaeva *et al.*, 2004) (see *Fig. 6*) was calculated. From the comparison of the powder patterns it can be concluded that complex (**I**) is easily oxidized to $Re_4O_6(OEt)_{10}$ analogous to the earlier studied isopropoxide derivative. It should also be noted that the Re_4-cluster core is not destroyed in the ambient atmosphere.
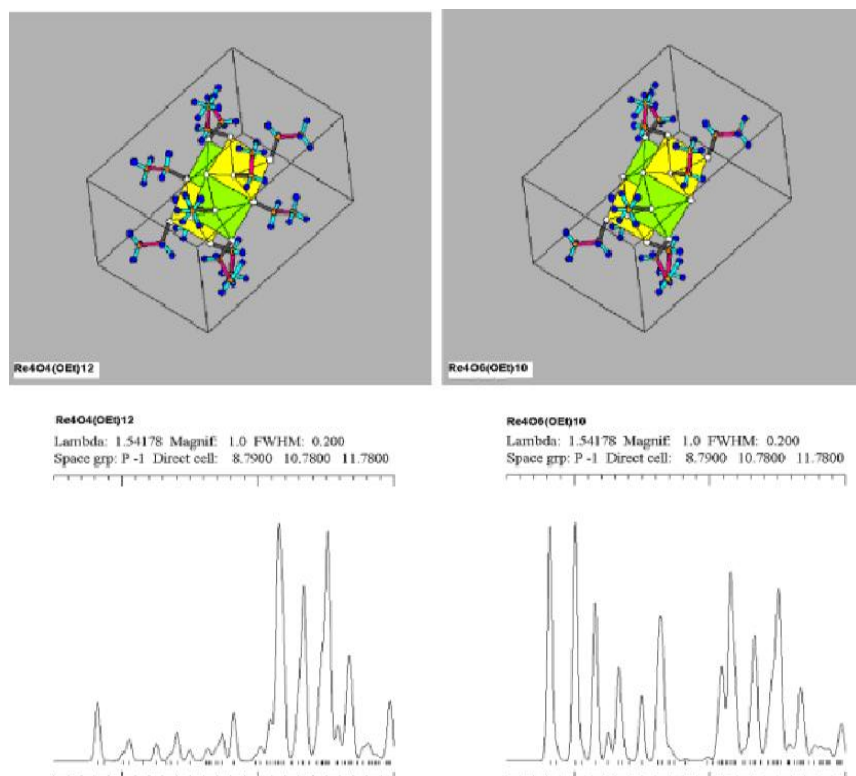
Figure 6. The molecules of $Re_4O_4(OEt)_{12}$ and $Re_4O_6(OEt)_{10}$ in the unit cell and the resulting theoretical X-ray patterns, generated by ATOMS software (ATOMS for Windows 2006)

The complex (**I**) was annealed at three different temperatures in N_2 atmosphere. The first sample (at 250 °C) reacted spontaneously with air forming a white smoke. The second sample (heated up to 300 °C) was black in color and was amorphous. The last sample (450 °C) showed metallic luster and seemed to be stable to air. The TG curve showed that the decomposition occurred in two steps, where the first one was connected with loss of Re_2O_7 together with organic part of the complex (**I**), and the second with loss of the rest of carbon as CO_2 (see Fig. 4 in Paper I). The total weight loss is corresponding to formation of the rhenium metal.

In case of bimetallic complexes the increasing size of the ligand is also influencing the bond lengths in all the complexes, which is confirmed by the IR – spectra and by the results of solution and refinement of the structures (see Figs. 2, 3 in Paper III and *Table 3*). The bond lengths increase in the following order:

40

r(Re–O)term < r(Re–O)μ < r(M–OR)term < r(M–O)μ < r(M–OR)μ < r(M–O–Re)μ.

It should also be mentioned that the same trend was observed even for the $Nb_4O_2(O^nPr)_{14}(ReO_4)_2$ complex.

Table 3. *IR − spectra of bimetallic complexes of common formula $M_4O_2(OR)_{14}(ReO_4)_2$ (M = Nb or Ta, R = Me, Et)*

Compound	IV	II	V	III	Vibration
IR–spectra recorded in Nujol		1277 w br			
	1146 w br		1151 w	1132 sh	ν (C–O) + δ (C–H)
	1097 w br	1099 m br	1114 m	1108 m br	
	1062 sh	1068 m		1076 m	
		1020 sh		1018 m br	
			996 m br		ν (Re=O)
	930 s	932 s	933 s	936 s	ν (M–O–M)
	889 sh	892 sh	901 sh	892 sh	
		878 m		876 m	
	807 m br	814 s	810 s br	810 s	ν (C–C)
	768 sh		772 m	772 w	δ (C–H)
	722 m	722 w			
	571 m	599 w	569 sh		ν (M–OR$_{term}$)
	526 m	536 m br	507 s br	527 w	ν (M–OR$_{bridg}$)
				479 w	
		478 w br		478 w br	ν (Re–OR$_{bridg,term}$)+δ (C–C)
IR–spectra recorded in HCB	1917 w	1915 w br	1915 w	1917 w	ν (C–C) + δ (O–H)
	1792 w				
	1634 w	1634 sh	1634 w	1634 w	
	1611 s	1611 s	1611 s	1611 w	
	1564 s	1564 s	1564 s	1564 w	
		1470 m		1473 sh	
	1452 s br		1455 m br	1445 m	
			1399 w	1407 sh	
		1379 m	1379 w	1383 s	
		1356 sh		1358 sh	
		1276 w			

Thus, the ligand size and crystallization temperature affect the crystallographic parameters and the position and geometry of perrhenate group, and also the bond lengths in the bimetallic complexes of common formula $M_4O_2(OR)_{14}(ReO_4)_2$, where M = Nb or Ta, R = Me, Et, ^nPr.

In addition, it was established, that the ethoxide complexes in contrast to methoxide ones have good solubility in hexane, toluene and other non-polar solvents, which makes them attractive precursors of complex oxide coatings for catalytic applications. The decisive role in solubility is played, evidently, by the size of the alkoxide ligand.

To confirm that the bulk samples of bimetallic complexes have the same structure as their single crystals the NMR analysis was performed (see Paper II and VI). The NMR spectra showed that the same molecular structures are present in the solutions.

All complexes were characterized by the thermo gravimetric analysis, which showed that the character of TG curves is the same for (**II**), (**III**) and (**IX**). As an example, one can consider in detail the thermal decomposition of $Ta_4O_2(OEt)_{14}(ReO_4)_2$ (**III**) in the nitrogen atmosphere. The first sample of (**III**) was decomposed by heating to 700 °C with a heating rate 5 °C/min, producing dark amorphous powder with considerable content of organic residue (**III**). Only approximately 1 wt% rhenium was conserved in the sample according to the EDS analysis. Therefore, it was necessary to design a process of thermal treatment in such a way, that Re would be conserved in the final product and result in improved crystallinity. First, the sample was pretreated by heating to 150 °C with a heating rate 5 °C/ min in nitrogen atmosphere with purpose to conserve Re and remove partly the organic part of the complex. The second step was thermal treatment of this sample on heating to 700 °C with the same heating rate followed by calcination for 30 h in nitrogen atmosphere. The two steps of mass loss were observed in the TG curve. The first one corresponds to decomposition of the complex together with some losses of Re_2O_7 and the second one to the loss of Re_2O_7, CO_2 and rest of organics. The total mass loss is 39.82% and corresponds to formation of $2Ta_2O_5 \cdot ReO_4$, in agreement with the theoretical value 39.87%.
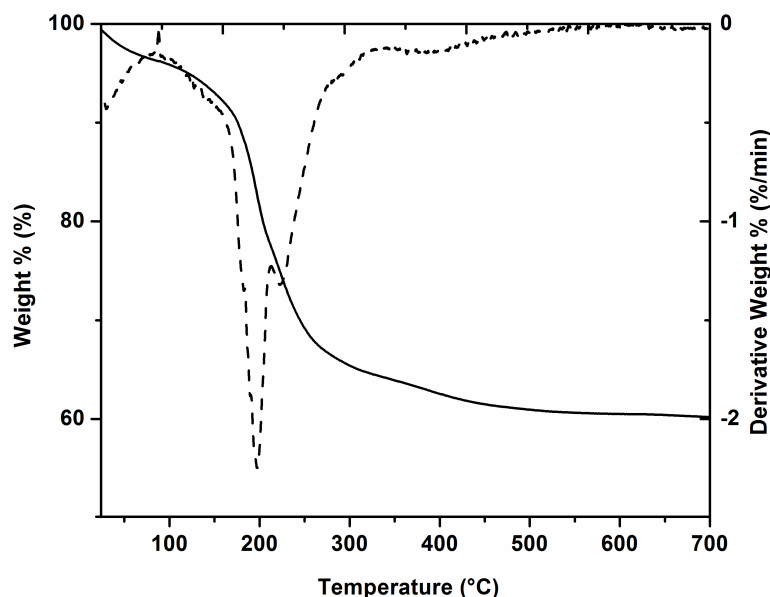
Figure 7. TGA curve for the thermal decomposition of $Ta_4O_2(OEt)_{14}(ReO_4)_2$ (**III**)

IR – spectra recorded in Nujol for trimetallic methoxocomplexes (**VI**) and (**VII**) are in agreement with the molecular structure. For all complexes the absorption bands were found in the same region. This confirms that all complexes have the same structure (see Table 03 in Paper IV). Because the Nujol peaks appear in the same region $1300 - 1700 \text{ cm}^{-1}$ as the stretching and bending vibrations of C–C, C=C, O–H for the all samples, the spectra were recorded also in HCB. The peaks of methoxo groups are clearly seen in these spectra for all samples (see *Table 4*).

It should be mentioned, that the bond lengths for all samples are approximately the same, only for the complex (**VIII**) a slight shortening of M–O bonds is observed connected, probably, with the ratio between Nb and Ta, and also less disorder in the structure (see Table 2 in Paper IV).

Moreover, the increasing size of the alkoxide ligand influences also the M–O bond energy, which is confirmed by analysis of the IR spectra (see Table TS2 in Paper VI). They show that the peaks shift toward smaller wavenumbers, which indicated that the interaction energy in case of trimetallic (**IX**) is lower than in methoxo complexes (**VIII**). For identification and characterization of the bulk samples of trimetallic species

43

(**VI)** and (**VII**), the XRD and SEM–EDS analysis of powder of the initial complexes was carried out (see Figs. 2-4 in Paper IV).

Table 4. *IR − spectra of $(Nb_xTa_{x-1})_4O_2(OMe)_{14}(ReO_4)_2$ (x = 0.3, 0.5, 0.7)*

Compound	VI	VIII	VII	Vibration
IR − spectra recorded in Nujol			1160 sh	ν (C–O) + δ (C–H)
	1109 s br	1117 m br	1106 m br	
	995 m br	994 w br	995 m br	
			941 m	ν (Re=O)
	930 s	929 m	927 w	ν (M–O–M)
	890 w br	893 w br	897 w	
	805 s br	807 m br	807 m br	
	721 w	720 w	720 w	δ (C–H)
	567 m br	564 w br	560 w br	ν (M–OR_term)
	516 m br	512 w br	533 sh	ν (M–OR_bridg)
			496 w br	
IR- spectra recorded in HCB	1633 w	1631 w	1628 w	ν (C–C) + δ (O–H)
	1607 m	1604 m	1610 m	
	1561 s	1561 s	1561 s	

The powder patterns (see Figs. 2 and 3 in Paper IV) of the initial trimetallic complexes (**VI**), (**VII**) display rather narrow peaks indicating high crystallinity of the samples. All reflections can be indexed in the unit-cell parameters characteristic of the complexes, which confirms the phase purity of the obtained products. Since complex (**IX**) is not stable to ambient atmosphere the NMR spectrum was recorded, which show that in the solution contains the same species (see Paper VI).

The SEM study of the powder of initial complexes (**VI**), (**VII**) and (**VIII**) showed that all samples have well formed crystalline appearance (see *Fig. 8*). Different shapes and sizes of crystals for all complexes can be seen in the SEM micrographs caused supposedly by different crystallization preferences revealed for different compositions.
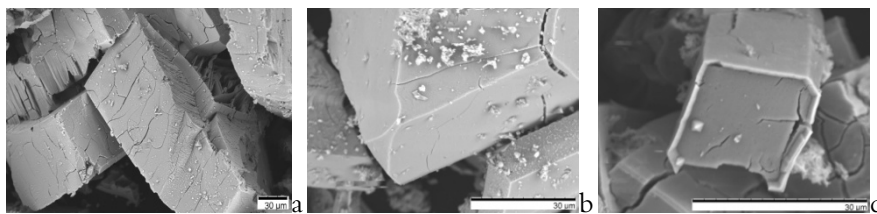
Figure 8. The SEM micrographs a – **VII,** b – **VIII**, c – **VI**

The EDS analysis shows (see Table 4 in Paper IV) that the crystallization of all complexes from solutions proceeded unevenly, probably because of the partial formation of the individual $(Nb_{0.5}Ta_{0.5})_2(OMe)_8(ReO_4)_2$ as impurity (Shcheglov P.A. *et al.*, 2002). Some crystals have relatively higher and some—lower Nb:Ta ratio compared with the average values imposed by the conditions of synthesis. The average ratios between Nb, Ta and Re were approximately the same for the samples of (**VI**), (**VII**) and (**VIII**) and for the isolated single crystals. For complex (**IX**) such tendency was not observed and the EDS analysis showed the same ratio between Nb and Ta as in the single crystal (see Table TS1 in Paper VI).

Complexes (**VI**), (**VII**) and (**VIII**) were subjected to thermal decomposition in air on heating up to 1000 °C with the heating rate of 5 °C/min. TGA revealed three steps in decomposition for all complexes. All samples displayed white-yellowish color and were stable on storage. The first step, apparently, is connected with the thermal decomposition of the complexes. The values of weight loss after the first step are close to the theoretical values, corresponding to the products presented in Table 5 in Paper IV. The second step, occurring on heating above 500 °C, is connected with the evolution of Rhenium heptoxide (Re_2O_7(g)) into the gas phase. The final products of trimetallic methoxocomplexes decomposition are solid solutions of Nb and Ta oxides with various compositions.

The thermal decomposition of (**VI**), (**VII**), (**VIII**) and (**X**) in nitrogen atmosphere on heating to 950 °C and 850 °C with the heating rates 10 °C/min and 5 °C/min, respectively, has been investigated as well. The TGA revealed two steps of weight loss (see Fig. S4 in Paper IV and *Fig. 9*). All samples displayed gray metallic color and were stable in ambient atmosphere.
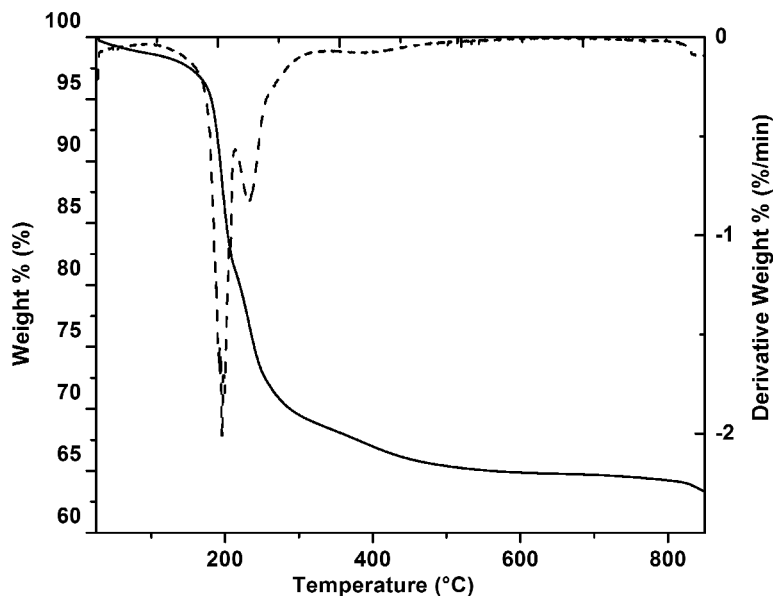
Figure 9. The TGA curve for thermal decomposition of $(Nb_{0.6}Ta_{0.4})_4O_2(OEt)_{14}(ReO_4)_2$ (**X**)

As it was described above, these two steps are connected with decomposition of the complex (**X**) at first and second with a loss of Re_2O_7 in the rests of organic part combined with process of carboxylation. The TGA curve (*see Fig. 9*) shows the total weight loss of 37.39%, which corresponds well to the theoretical value 37.62% calculated for the formation of $Nb_{2.4}Ta_{1.6}O_5 \cdot Re_2O_5$ from complex (**X**).

5.2 Preparation of Metal and Complex Oxide Materials

5.2.1 Preparation of Rhenium Metal

In **Paper I**, $Re_4O_4(OEt)_{12}$ was used as precursor to obtain nanoparticles of Rhenium metal. As we mentioned earlier, the X-ray powder analysis shows that complex (**I**) is not stable in the ambient atmosphere.

The complex (**I**) was annealed at 450 °C temperature in N_2. After thermal treatment the sample showed metallic color and seemed to be stable to air. The final product was investigated by XPD analysis and showed the formation of Re metal particles according to ICDD data (№ 05-0702) for Re metal. TEM studies of the products showed that the product obtained at 450 °C consisted of strongly agglomerated nanocrystals approximately 3 nm

in size (see *Fig. 10*). EDS analysis in TEM confirmed that the sample consisted of Re.
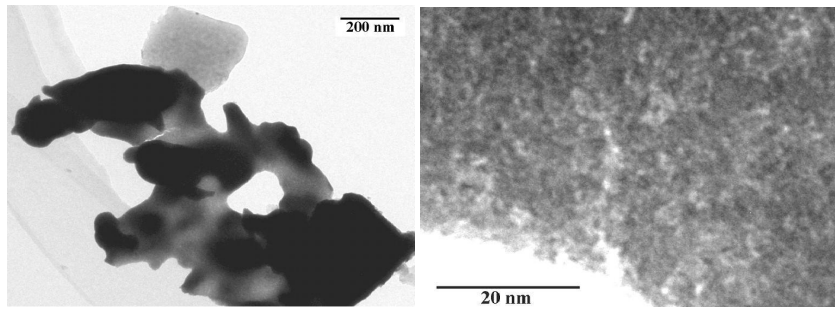

Figure 10. TEM micrographs of Rhenium oxoethoxide heated at 450 °C, in N_2.

Thus it has been established that the thermal decomposition of $Re_4O_4(OEt)_{12}$ proceeds in a principally different way compared to $Re_4O_6(OMe)_{12}$ and $Re_4O_6(O^iPr)_{10}$. For the last two complexes ReO_3 was the only product of the first step in decomposition, and it transformed further into ReO_2 stable to at least 800 °C (Kustov *et al.*, 2004b; Kustov *et al.*, 2004a). Rhenium metal could be obtained from methoxide or isopropoxide only using hydrogen gas as reductive agent at the temperature of 380 °C. Transformation into metal on heating in the inert atmosphere, without introduction of any reductive agent, makes Rhenium ethoxide, $Re_4O_4(OEt)_{12}$, an attractive precursor of Rhenium nanopowder material for deposition into mesoporous templates such as Al_2O_3, Nb_2O_5 or Ta_2O_5.

5.2.2 Preparation of porous complex oxides

The preparation of oxide materials from the trimetallic oxomethoxo complexes based on Nb, Ta and Re with the ratios between Niobium and Tantalum 0.3, 0.5, 0.7 can be successfully achieved as presented in the Paper IV.

After the thermal decomposition in air, the products of heat treatment were investigated using powder XRD and SEM-EDS. The samples of the decomposition products reveal narrow and very closely situated reflections, indicating high crystallinity (see Fig. 5 in Paper IV). According to the results of powder XRD analysis for the investigated compositions $(Nb_{1-x}Ta_x)_2O_5$, where x = 0.3, 0.5, 0.7, it was concluded that isomorphous replacement of Nb with Ta increased the temperature stability domain of the of L(γ)-modification–related M_2O_5 phase up to 1000 °C. These data confirm the formation of solid solutions of Niobium and Tantalum oxides $(Nb_{1-x}Ta_x)_2O_5$

on the decomposition of trimetallic complexes $(Nb_{1-x}Ta_x)_4O_2(OMe)_{14}(ReO_4)_2$, where x = 0.3, 0.5, 0.7.

The SEM investigation shows that all the products of decomposition have a crystalline, semi-ordered porous structure (see *Fig. 11*) with size of the pores 100–250 nm. Based on the SEM micrographs of initial complexes and their products of decomposition (see *Figs. 8* and *11*) it was confirmed that crystals kept the form and showed a high stability to high temperature treatment (1000 °C).
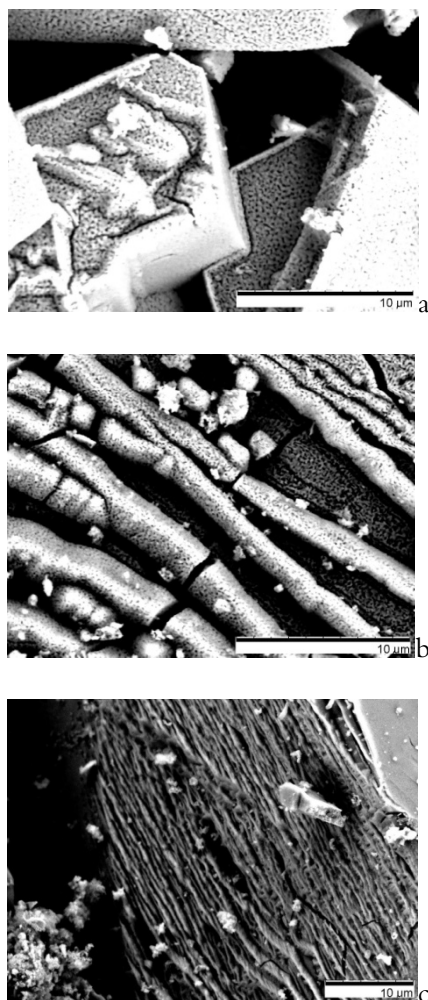

Figure 11. The SEM micrographs the products of decomposition in air: a – $(Nb_{0.7}Ta_{0.3})_4O_2(OMe)_{14}(ReO_4)_2$; b – $(Nb_{0.5}Ta_{0.5})_4O_2(OMe)_{14}(ReO_4)_2$; c – $(Nb_{0.3}Ta_{0.7})_4O_2(OMe)_{14}(ReO_4)_2$

The EDS analysis shows that the ratio between Nb and Ta is changed for the samples (**VI**) and (**VII**), which is probably connected with the higher volatility of Niobium alkoxide derivatives compared to Tantalum ones as confirmed by the mass-spectral investigation. An analogous relation in relative volatility of Niobium and Tantalum components in a complex has earlier been observed in the classic work of L.G. Hubert-Pfalzgraf on bimetallic Niobium − Tantalum alkoxides (Hubert-Pfalzgraf *et al.*, 1978). Hence, it was noted that the thermal decomposition of trimetallic oxomethoxo complexes (**VI**), (**VII**) and (**VIII**) opened an approach to formation of solid solutions of complex porous oxides based on *L −* modification of Ta_2O_5 of common formula $(Nb_{1-x}Ta_x)_2O_5$, where *x = 0.3, 0.5, 0.7.*

It was observed that volumes of the unit cell for Nb:Ta = 50:50 and the pure pentoxide of Tantalum Ta_2O_5 were practically identical, while for the intermediate Nb:Ta compositions = 30:70 the cell volumes were essentially bigger. It was suggested that intermediate compositions were characterized by more disordered arrangement of cations.

For the complexes (**VI**) − (**VIII**) the thermal decomposition was also carried out in N_2. The results of TG analysis show that all samples contained traces of Rhenium, which is confirmed by assignment of indices in the XPD patterns. The results of unit cell parameters calculation (see Table 8 in the Paper IV), based only on peaks with strong intensity, showed for $(Nb_{0.7}Ta_{0.3})_4O_2(OMe)_{14}(ReO_4)_2$ that the sample contained a phase related to monoclinic *H* - Nb_2O_5 modification. The patterns obtained for the samples derived from complexes (**VII**) and (**VIII**) contained a phase related to the *L*-modification of Ta_2O_5 (see Fig. 5 in Paper IV). It is connected, most likely, with the fact that enters more Niobium than Tantalum into the structure of the complex (**VI**). Hence, changing the ratio between Niobium and Tantalum it is possible to control the phase composition in relation to modifications related to the known structure types of Nb_2O_5 or Ta_2O_5.

Thus, the thermal decomposition in air of all the studied complexes $(Nb_{1-x}Ta_x)_4O_2(OMe)_{14}(ReO_4)_2$ (x = 0.3, 0.5, 0.7) leads to solid solutions related to the block structure of *L*-modification of Ta_2O_5 at the temperatures < 1000 °C with semi-ordered macro porous structures, where the size of pores lies in the range 100-250 nm. The thermal decomposition in dry nitrogen provides solid solutions related to the block structures of the *H*-modification of Nb_2O_5 for the Niobium-rich precursors and the *L*-modification of Ta_2O_5 for Ta:Nb ≥ 1:1 at the temperature < 1000 °C (see Fig. S5 in Paper IV).

5.2.3 Nanobeads

The spherical aggregates were obtained by two types of hydrolysis: natural and accelerated. Bi- and trimetallic complexes of common formula $(Nb_{1-x}Ta_x)_4O_2(OR)_{14}(ReO_4)_2$, where x = 0–1 and R = Et, ^nPr subjected to both types of hydrolysis. Due to poor solubility of methoxocomplexes (**IV**), (**V**) and (**VIII**) the preparation of nanobeads was hindered. During both types of hydrolysis no significant loss of rhenium was observed (see Paper VI).

For all the tested precursors the hydrolysis produced mostly spherical beads with different degree of aggregation. Relatively small fraction of bigger poorly shaped aggregates was also present. The size of the spheres was mostly uniform and showed no trend in relation to either nature of the alkoxide ligand or to concentration of the precursor solution.

From SEM study it can be seen that all nanobeads formed by natural hydrolysis have dense oxide surface based on Nb or/and Ta metal oxides, resulting in very low active surface as measured by nitrogen sorption (*see Fig. 12*).
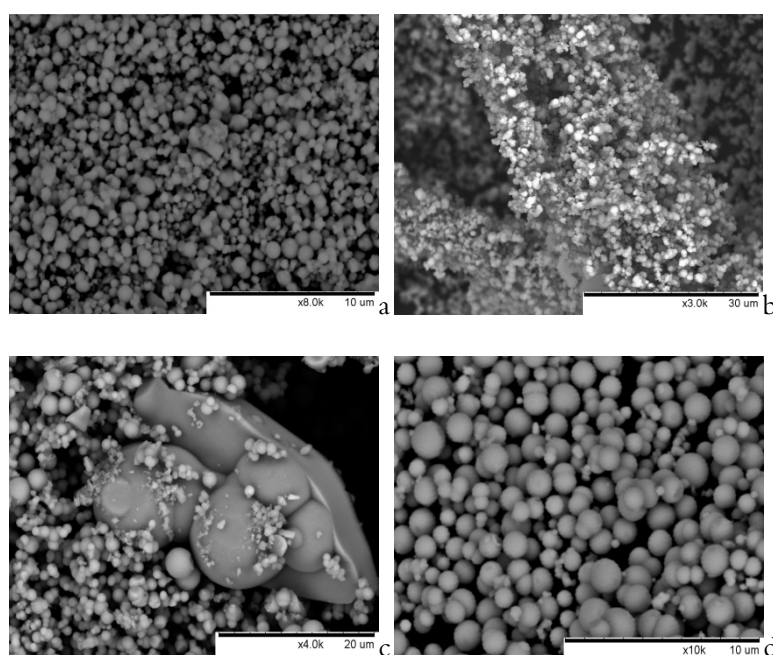

Figure 12. SEM images of nanobeads obtained by natural hydrolysis: a – **NBI** from (**X**), b – **NBIII** from (**IX**), c – **NBIV** from (**II**), d – **NBVI** from (**III**)

The different size of samples could be explained by the different nature of Nb and Ta metal oxides, specifically higher electronegativity of Nb,

resulting in lower negative charge density on the perrhenate ligands and less efficient structure-directing action. The sample **NBI** reveals almost the same size of well-shaped spheres approximately 500–700 nm in average (*see Fig 12*), mostly not aggregated. In case of spherical particles from the bimetallic precursors it can be noted that niobium-containing ones distinctly are not uniform and have different size starting from 1μm and up to more than 40 μm. The tantalum-containing sample **NBVI** shows well-formed, practically uniform particles 500 nm to 2 μm in size, even when the solution concentration is quite high. The EDS analysis showed that after hydrolysis ratios between Nb or/and Ta and Re remain almost the same in compared to starting materials (see Table 1 and Table TS1 in the Paper VI).

The FT-IR investigations of all nanobeads show the presence of Re as perrhenate group, ReO_4^-, which is confirmed by the presence of the characteristic Re=O bands in the range 900–950 cm^{-1} (*see Table 5*).

Table 5. *Comparison of the FTIR spectra of the nanobeads obtained by natural hydrolysis*

	NBI	NBIII	NBIV	NBVI
ν(M–O)			410 w	
ν(M–O–M)			422 w	
		495 w br	465 w br	
	516 sh		502 m br	513 w br
		587 s	570 s br	
	638 s			640 s br
ν(M–O–Re)		719 w	730 w br	
	813 m br	820 m br	802 w br	813 m br
			839 w br	
ν(ReO_3) belongs to ReO_4^-	909 w	909 s	911 w	909 w
	931 sh	930 m br	931 w br	
	939 s br	946 sh	947 w	942 s br

One of the most important indications provided by IR spectra is the presence of vibrations, corresponding to the Nb(Ta)–O–Re stretching mode at $700 - 800$ cm^{-1}. It should be noted that almost at the same wavelength these vibrations for the initial complexes were observed (see *Table 5* and Table TS2 in the Paper VI). The vibrations at $400 - 650$ cm^{-1} correspond to Nb(Ta)–O–Nb(Ta) stretching mode, which is in agreement with starting materials. The coordination of metal centers does not change during the

hydrolysis as indicated by EXAFS spectra (see Fig. S7–S10 in Paper VI), i.e. for Nb(Ta) remains octahedral and for Re tetrahedral.

The accelerated hydrolysis is resulting in the formation of spherical particles with size and degree of aggregation strongly dependent on the polarity of the solvent (see Fig. 2 in the Paper VI). The kinetics of aggregation of the initially formed primary particles was followed by laser reflection microscopy using NanoSight (NTA Version 2.1) instrument (see real-time video VS1 and reports S11, S12 in the Paper VI). The initial particles with the size below 10 nm aggregated uniformly to spherical particles of several hundred nm in size within minutes. The aggregates can be split into initial small particles again by sonication in a standard ultrasound bath in 5 min and the re-aggregation can then be followed to occur reproducibly with formation of again same type spherical aggregates in the same time scale. This is an important evidence for the formation of the observed oxide particles through so called Micelle Templated by Self-Assembly of Ligands (MTSAL) mechanism (Seisenbaeva *et al.*, 2010; Kessler, 2009; Seisenbaeva *et al.*, 2008; Kessler *et al.*, 2006).

From the SEM study of nanobeads formed by the accelerated hydrolysis it could be seen that the addition of the parent alcohol to the system leads to formation of better formed nanobeads, while the hydrolysis only with water results in the particles with smaller size and less developed shape (see Fig. 2 in the Paper VI). The bigger aggregates are absent, because the coalescence of the primary particles occurs more uniformly as the distribution of water in the volume is more uniform due to agitation. Even in this case the retention of Re is complete and occurs in the form of ReO_4^- ligands according to EDS and FTIR.

In spite of well-defined geometry of the metal centers, the produced nanobeads remain amorphous on thermal treatment up to 700 °C even after 24 h. Increasing the temperature to 1000 °C leads to complete loss of Re with formation of crystalline porous nanobeads based on only Nb or/and Ta oxides (*see Fig. 13*).
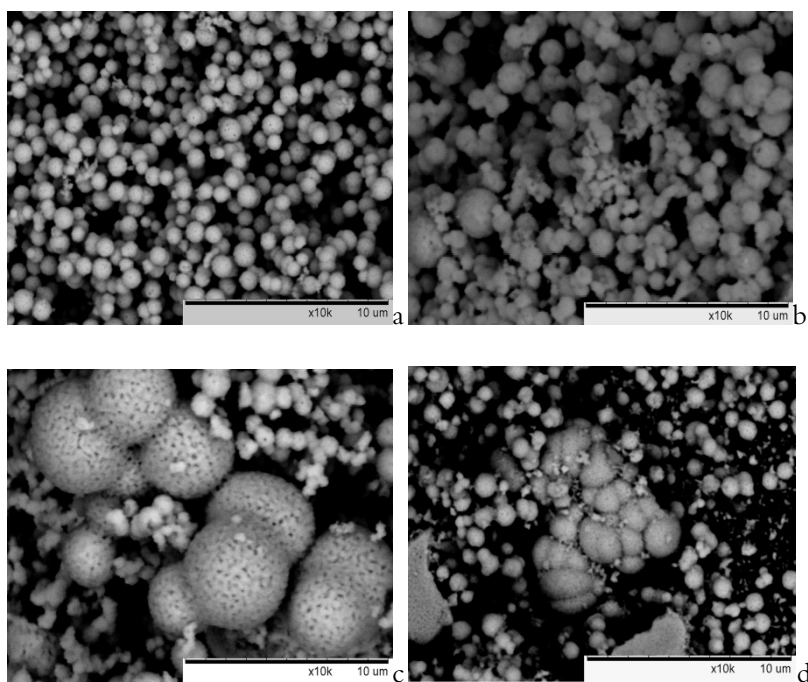
Figure 13. SEM images of porous nanobeads a – **NBI**, b – **NBIII**, c – **NBIV**, d – **NBVI**

The XPD analysis of the thermally treated products (see Fig. 4 in the Paper VI) showed that the structure of **NBIII** and **NBIV** samples related to the block structure of monoclinic α-Nb_2O_5 modification, while for the samples **NBI** and **NBVI** the formation of the orthorhombic modification γ-Ta_2O_5 is registered.

5.3   Catalytic applications

5.3.1 Characterization of the obtained catalysts

Catalysts were obtained by impregnation of TiO_2 support with $Re_4O_4(OEt)_{12}$ and $Ta_4O_2(OEt)_{14}(ReO_4)_2$ alkoxide solutions with subsequent thermal treatment in air on heating to 300 °C for 2 h with heating rate 5 °C/min. In both steps, as it was expected, some losses of Re occurred presumably as Re_2O_7, due to the volatility of this oxide, and also of organic part of the complexes.

After thermal treatment all obtained catalysts were characterized by SEM–EDS analysis. First the surface of the cylinders was investigated (*see Table 6*). The results corresponded in average to expected contents except

for **S5**, where the higher amount of Ta compared to the calculated one was detected on the surface.

Table 6. Results of EDS analysis of the catalysts

	Ti		Ta		Re	
	wt%	*at%*	*wt%*	*at%*	*wt%*	*at%*
S1	99.01±2.08	99.74±2.09			0.99±0.03	0.26±0.01
S2	98.08±2.05	99.51±2.09			1.88±0.05	0.49±0.01
S3	61.51±1.29	85.81±1.80	34.99±0.98	12.94±0.36	3.47±0.10	1.25±0.04
S4	62.57±1.31	86.25±1.81	28.97±0.81	10.80±0.30	9.75±0.27	2.94±0.08
S5	85.99±1.81	95.86±2.01	14.01±0.39	4.14±0.12		

To be able to understand the phenomenon described above a cross over cut of catalysts/TiO_2 cylinders was made followed up by EDS analysis (*see Fig. 14*).
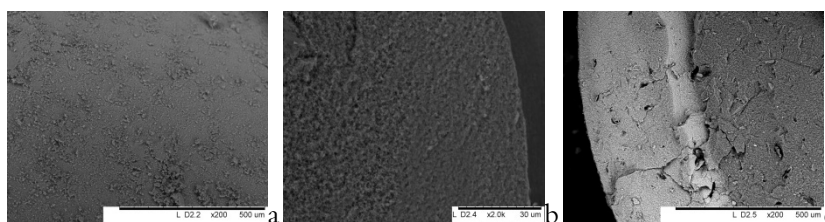
Figure 14. SEM images: a – surface of the **S2**; b – cross over cut of **S4** and c – cross over cut of **S5**

In case of **S1** and its analog **S2** it was found that the ReO_x species were not uniformly distributed in the volume of TiO_2 cylinders. However, in the case of **S3** and **S4** better homogeneity was observed in the distribution of $TaReO_x$ species in the whole volume of the TiO_2 cylinders, while in case of **S5** the TaO_x species were deposited closely to the surface with an impregnation depth of about 300 μm (*see Fig. 14c* – bright area due to heavy element contrast).

The observed difference in the deposition of the material can be explained in view of the different reactivity of the alkoxide precursors in relation to crystallization and hydrolysis–polycondensation, and different nature of starting materials.

FTIR investigations were performed to determine the chemical groups present in the catalysts. Since TiO_2 has in the IR spectra a big broad band between 400 cm^{-1} and 880 cm^{-1} all spectra were normalized and the TiO_2 phase signal was subtracted to reveal the peaks corresponding to loaded catalysts. After the fitting procedure the positions of the peaks corresponding

to different Re–O and Ta–O vibrations were identified (see Table 2 in the Paper V).

In order to make differences between Re_2O_7 and ReO_4^- stretching modes the IR spectrum for rhenium heptoxide partially hydrolyzed to perrhenic acid was recorded (*see Fig. 15*)
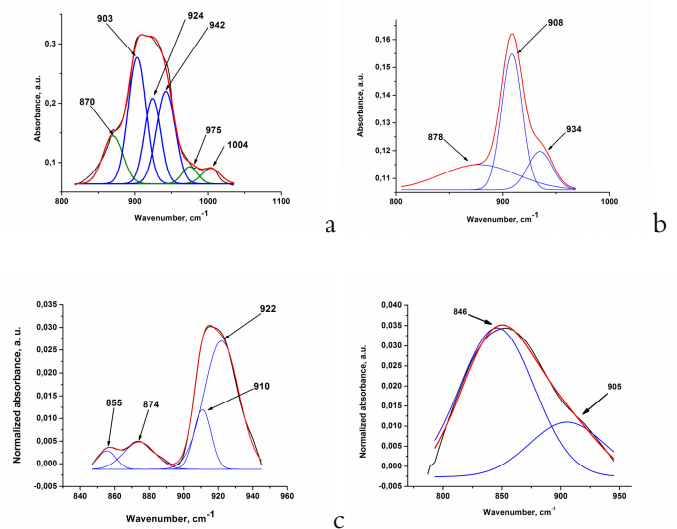

Figure 15. The FTIR spectra: a – oxidized Re_2O_7, b – $Re_4O_4(OEt)_{12}$, c – **S1** and d – **S2**

The bands at 870 cm^{-1}, 975 cm^{-1} and 1004 cm^{-1} could be assigned to Re_2O_7 according to (Beattie *et al.*, 1996), while the bands at 903 cm^{-1}, 924 cm^{-1} and 942 cm^{-1} belong to ReO_4^- group in compliance with (Mohammed & Sherman, 1981) (*see Fig. 13a*). In case of **S1** and **S2** the vibrations at 855 cm^{-1} and 832 cm^{-1}, respectively, are close to the Re–O–H stretching modes reported in (Mohammed & Sherman, 1981). Since the samples of the catalysts did not contain OH-bonds or perrhenic acid, those peaks could be assigned to the Re–O–Ti vibrations. Peaks at 870 cm^{-1} and 874 cm^{-1} for samples **S2** and **S1** respectively should be attributed to the Re–O–Re stretching mode, which is in good correlation with the peak at 878 cm^{-1} observed for the starting material $Re_4O_4(OEt)_{12}$ (**I**) and at 870 cm^{-1} for Re_2O_7 (*see Fig. 15*). The Re=O stretching modes for the $Re_4O_4(OEt)_{12}$ alkoxide complex are considerably different from those for the **S1** as well as **S2**, where the vibrations at 910 cm^{-1}, 922 cm^{-1} and 911 cm^{-1} could be assigned to vibrations of the perrhenate group ReO_4^- according to (Mohammed & Sherman, 1981) (*see Fig. 15*). The samples **S1** and **S2** contain a mixture of two different species, Re_2O_5 and ReO_4^-, according to

the IR spectra (*see Fig. 15*) and XPS results (see below) which can be explained by the properties of the $Re_4O_4(OEt)_{12}$ complex. The alkoxide precursor (**I**) contains rhenium in the oxidation state +V.

It should be noted that while for **S1** and **S2** both Re–O–Re and Re=O vibrations were detected, for **S3** and **S4** only the last one at 920 cm^{-1} was observed (*see Fig. 16*), at the same position as for the starting material, which can be explained by the preservation of the perrhenate unit already present in the precursor $Ta_4O_2(OEt)_{14}(ReO_4)_2$.
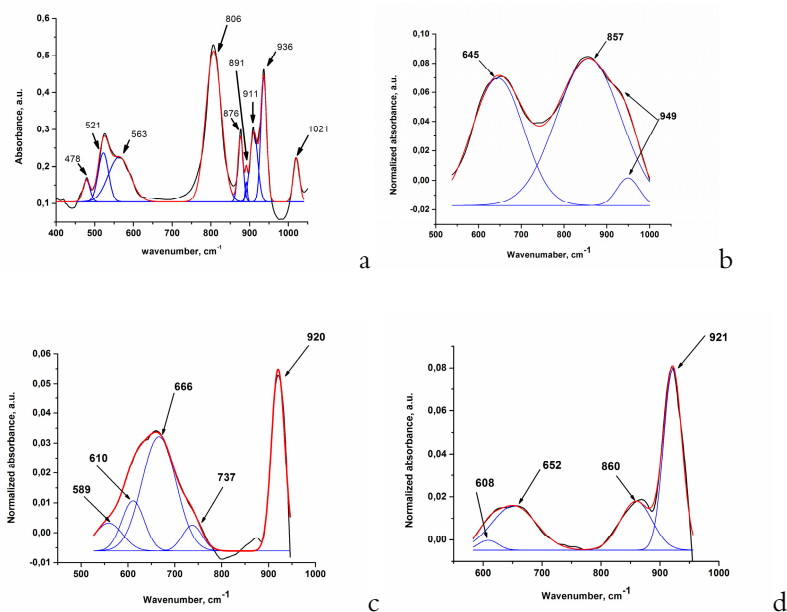
Figure 16. The IR spectra: a – $Ta_4O_2(OEt)_{14}(ReO_4)_2$, b – **S5**, c – **S3** and **S4**

As it can be seen from the IR spectra almost the same position of peaks of the Ta–O–Ta vibrations can be found for the **S3** and **S4** (*see Fig. 16c and 16d*). As expected, the vibrations for Ta–O–Re stretching modes could be observed at 737 cm^{-1} and 860 cm^{-1} for **S3** and **S4** respectively, which are in good correlation with bands for the staring material $Ta_4O_2(OEt)_{14}(ReO_4)_2$ (**III**) (*see Fig. 16a*).

For the catalyst **S5** three peaks have been detected corresponding to different types of vibrations: the first one at 645 cm^{-1} to Ta–O–Ta and two others to Ta–O, while the peaks observed for the precursor $Ta_4O_2(OEt)_{14}(ReO_4)_2$ (**II**) are situated at the range 478 – 563 cm^{-1} (*see fig. 16*). It should be mentioned that the appearance of the peak at 949 cm^{-1} indicates the presence of sub-oxides TaO and TaO_2 (Dharmaraj *et al.*, 2006).

In order to confirm the aforementioned hypothesis, the outer atomic layers up to 50Å were scanned using X-Ray Photoelectron Spectroscopy. XPS analysis exhibits almost the same composition for the samples **S1** and **S2** (see Table 3 in Paper V). The results obtained by XPS and EDS analysis showed a significant difference in content of the surface of the crystallites and the bulk samples (See Table 1 and 3 in Paper V). It could be confirmed that the external 50Å of the TiO_2 crystallites were poorer in Rhenium than the volume studied by EDS. The XPS spectra show that the rhenium atoms are present in oxidation state +V or +VI for outer shells of these two samples. The principal Re $4f_{7/2}$ component, located at 44.1 eV for **S1** and 43.7 eV for **S2** respectively, could be referred to Re_2O_5 or ReO_3 according to (Naor *et al.*, 2010). The slight shift could be explained by the lower content of Re in the **S2** sample. The peak positions for the Ti 2p and O 1s were at 458.8 and 530.1 eV respectively.

The sample **S5** showed an important quantity of 14 at% Tantalum at the surface. As expected, the BE corresponding to Ta $4d_{5/2}$ exhibited typically at 230.6 eV corresponding to Ta atoms in the oxidation state +V (Ho *et al.*, 1987).

Concerning the two other samples **S3** and **S4**, it seems that the catalysts have the $TaReO_x$ phases at the surface with Ta/Re ratios equal to 3.3 and 2.1 respectively. The thickness of the $TaReO_x$ layer increased as a higher quantity of each element (i.e. Ta and Re) was observed, correlating with the decrease of the Ti content analyzed by XPS (see Table 3 in Paper V). This indicated a better dispersion of the active phase on the surface of the TiO_2 support ((Re+Ta)/Ti = 0.6 and 0.1 for **S4** and **S3** respectively). The oxidation state of Re in these two samples is mainly +VII with a binding energy of the Re $4f_{7/2}$ equal to 46.3 eV corresponding to ReO_4^- (Naor *et al.*, 2010), a minor contribution of Re +VI is clearly evidenced for the sample **S3** by a peak at 44.4 eV corresponding to ReO_3. To prove the presence of Re +VI is not straightforward on the **S4** sample. The Ti 2p and O 1s photopeaks occurred in the typical areas for TiO_2 at 459.0 eV and 530.2 eV respectively.

Moreover, all catalysts were characterized by XPD and TEM analysis. In the X-ray powder patterns all samples were represented mainly by anatase form of TiO_2. Only some extra peaks identified in fig. 5 – Paper V could be referred to catalytic phases in the samples (see Fig. 5 in Paper V). Furthermore, the XPD results have indicated that the grain size of crystallites of the catalysts decreased with the loading of catalysts onto the support. From the TEM images it can be seen that particles are present as agglomerates. Figure 6 displays a representative TEM images for **S1** and **S4**

samples. The SAED image analysis shows polycrystallinity of the samples, which made it difficult to determine the structure of the catalyst phase (*see Fig. 17*).
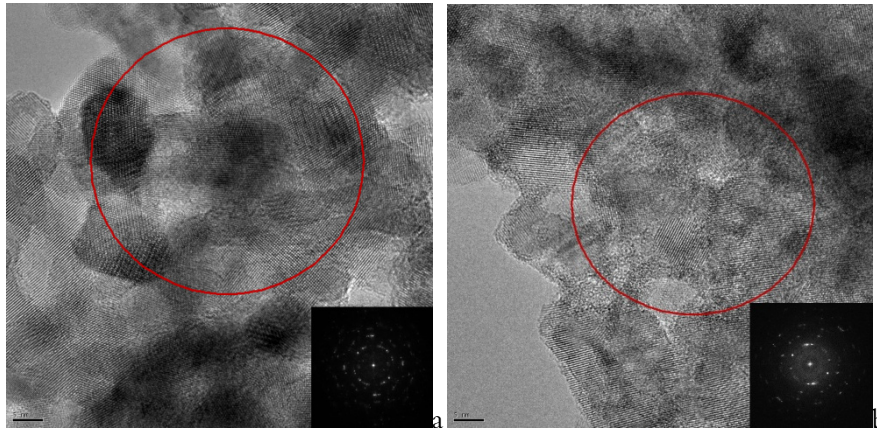

Figure 17. HRTEM images of **S1** and **S4** samples

Thus, the SEM investigation demonstrated that the distribution of the catalysts occurred in different ways. In fact, for the **S1** and **S2** the distribution of the precursor of ReO_x species, the $Re_4O_4(OEt)_{12}$ alkoxide, resulted in a difficulty in spreading them evenly in the whole volume of TiO_2 cylinders. On impregnation of TiO_2 cylinders the specific behavior of the precursor caused, in the case of **S5**, the formation of a dense TaO_x layer with a thickness of about 300µm. However, in the case of **S3** and **S4**, another trend resulting in better distribution through the volume of TiO_2 cylinders was observed. These phenomena could be explained by the nature and properties of the starting materials as described above. The FT-IR results demonstrated that all samples contained the perrhenate group ReO_4^-. According to IR spectra investigations the catalytic O_3Re-O group was connected to the TiO_2 support through the oxo–bridge in the of **S1** and **S2** samples. In the case of **S3** and **S4** the perrhenate group was connected through oxo-bridges to Ta atoms. Since in the Ta_2O_5/TiO_2 catalyst the Ta atoms were connected to the support through oxo-bridges, it is plausible to suggest that in the catalysts **S3** and **S4** the same type of connection is present. According to XPS data for **S1** and **S2** the Re atoms were present mainly in the oxidation state +V or +VI, while for the **S3** and **S4** samples they were in oxidation state +VII. Moreover it should be mentioned that ReO_x species were reduced onto the surface of the support. These

58

phenomena resulted in the appearance of extra peaks corresponding to rhenium in oxidation state +VI in the **S3** sample.

5.3.2 Catalytic activity

The methanol oxidation reaction (*see Fig. 1*) on all the catalysts was performed at 275 °C under poor and rich conditions with 7% and 40% of methanol respectively, diluted by air with an approximate flow of 40 ml/min. It was found that the conversions increased with the reaction temperature for each sample. Table 7 shows the catalytic results for all catalysts at the higher and lower methanol conversion. In each case the quantity of oxygen was enough and there were no limitations in performing oxidation reaction caused by low oxygen concentration. It could be seen that the activities for the two samples, **S1** and **S2**, were comparable revealing methanol conversion of 14% and 11% in the poor condition and 6.5% and 4% in the rich condition respectively. In this case the selectivity for both catalysts was mainly toward F at rich conditions (*see Table 7*).

Table 7. *Catalytic results*

Sample	MeOH vol (%)	Max MeOH conversion in (%)	MeOH conversion (mol)	S(F)	S(FM)	S(DME)	S(DMM)	S(CO)	S(CO$_2$)
TiO$_2$	7	6	0.42	41	17	42			
	40	4	1.6	49		44	7		
S1	7	14	0.98	41	17	28		13	1
	40	6.5	2.6	43	11	26	20		
S2	7	11	0.77	39	15	30		15	1
	40	4	1.6	37	13	30	17	2	1
S3	7	37	2.59	40	17	15		26	2
	40	15	6	15	17	12	52	3	1
S4	7	43	3.01	39	19	15	1	21	5
	40	23	9.2	6	13	11	67	1	1

It should also be noted that the CO$_x$ molecules were present in a non-negligible quantity especially in the poor methanol condition (*see Table 7*). On the contrary, when the quantity of methanol (rich condition) was increased, these molecules almost disappeared (*see Fig. 18*).
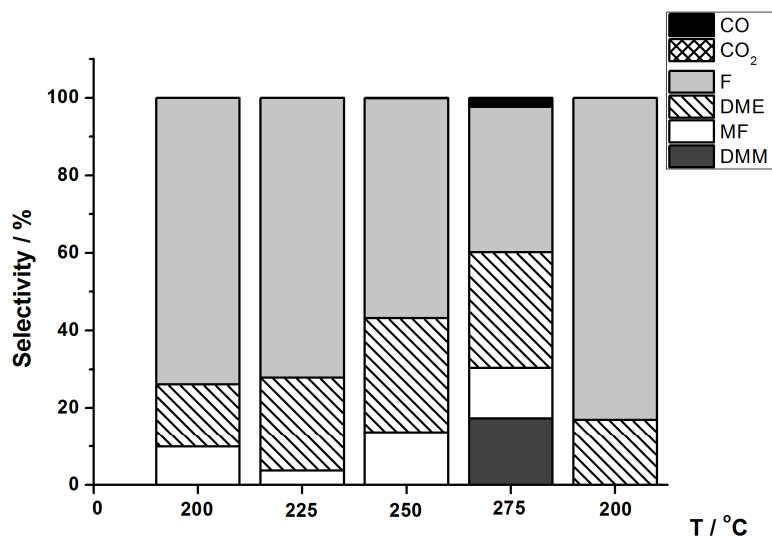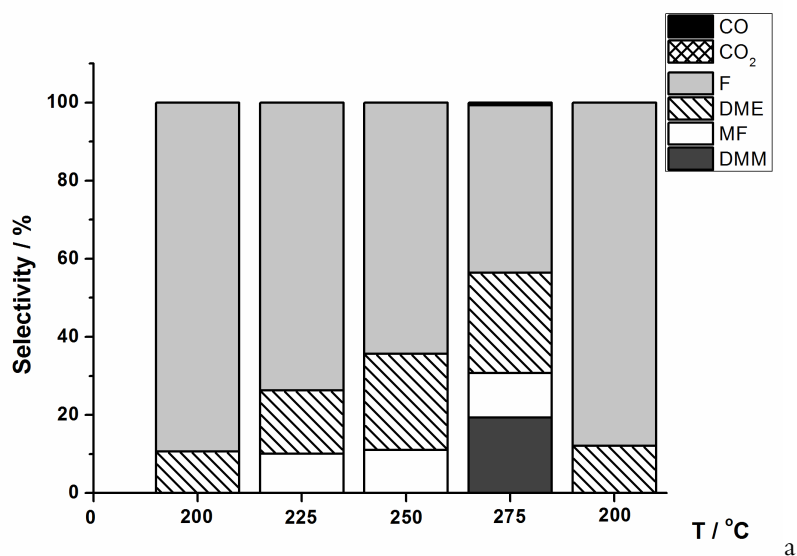
Figure 18. Selectivity of **S1** (a) and **S2** (b) function of temperature in rich methanol condition

For the **S3** and **S4** samples the main product at each temperature was DMM (*see Fig. 19*) in rich condition. It is worth noting that the selectivity increased with temperature up to 250 °C and then decreased. In order to verify the catalyst survival at the end of the experiment the decrease of the

temperature to 200 °C demonstrated an increase in DMM selectivity. The other detected products were MF, DME and F, with almost no trace of CO_x as evidenced in rich condition, while the opposite tendency was observed in poor condition (*see Table 7*).

a

b
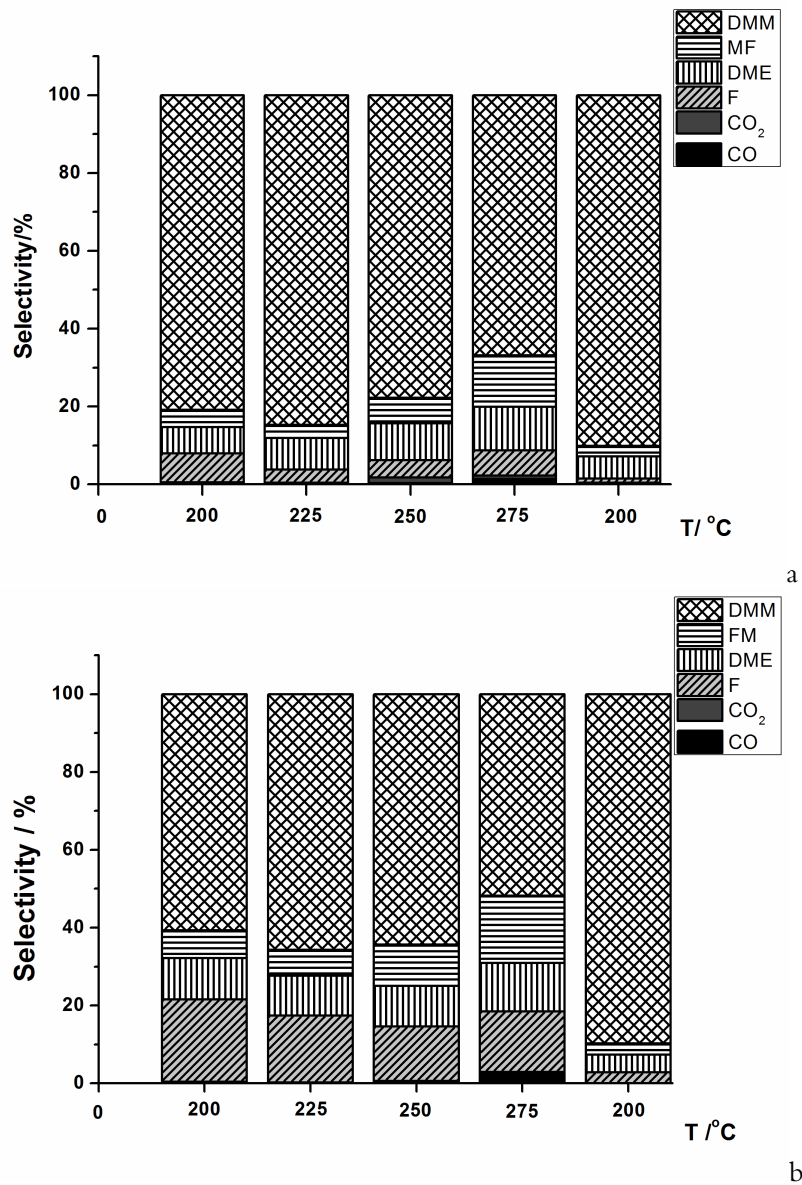
Figure 19. Selectivity of **S3** (a) and **S4** (b) function of temperature in rich methanol condition

It should also be noted that in case of 7% methanol conversions the selectivity of **S3** and **S4** was mainly towards formaldehyde and no DMM formation occurred.

This knowledge permitted to evaluate the redox and acidic properties of **S3** and **S4**. To be able to understand different properties of ReO_x/TiO_2 and $ReTaO_x/TiO_2$ catalysts, a Ta_2O_5/TiO_2 catalyst was obtained. The Ta atoms in **S5** effectively add acidic property to the support (main product is DME) without changing drastically the methanol conversion, which did not exceed 6% in rich methanol condition (*see Fig. 20*).
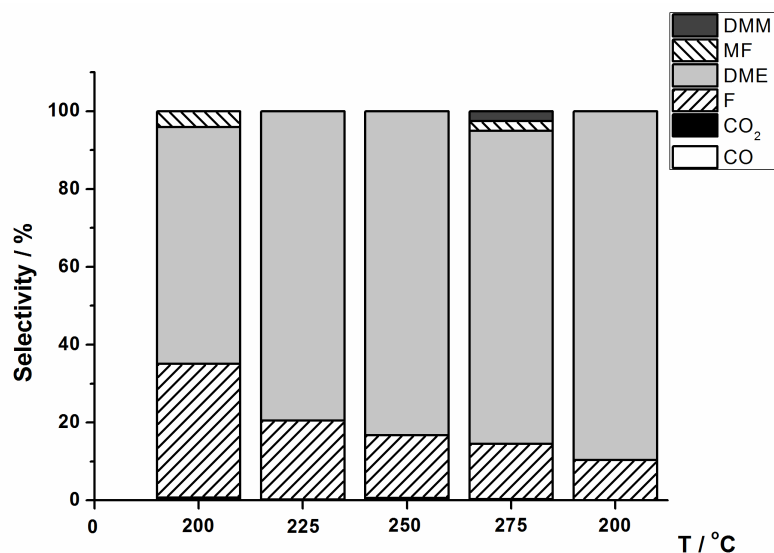
Figure 20. Selectivity of **S5** function of temperature in rich methanol condition

In terms of selectivity, the Re oxide species deposited on TiO_2 supports (**S1** and **S2**) appeared to have a good balance between redox and acidic properties in order to form DMM and MF, which were not present at all or were formed in very small quantities for the TiO_2 support alone. According to table 4, the methanol conversion decreased with the rhenium loading in poor and rich methanol conditions for **S3** and **S4**. In terms of selectivity, in the poor methanol condition, the main product was formaldehyde (SF ~40%), meaning that the redox properties were dominant under this condition or that the adsorption energy was lower than the one needed to process to the dehydration/condensation reaction producing DMM. Nevertheless, the presence of MF seems to be proof that the redox/acidic

properties were revealed simultaneously in these catalysts. Increase in the quantity of methanol in the feed, resulting in the increase in probability of higher methanol adsorption on the surface of the catalysts, favours condensation of formaldehyde with methanol producing DMM. Table 7 shows that DMM selectivity reaches more than 50% for both **S3** and **S4** samples. At the same time the selectivity towards F decreases drastically, which seems to be in agreement with our previous assumptions. The mixed oxidation numbers +VI and +VII for Rhenium in the **S3** and **S4** samples increased drastically the DMM selectivity under rich methanol condition. It agrees with the assumption claimed by Iwasawa et al(Yuan *et al.*, 2000b). The fact that the two oxidation states are present in the catalysts permits the formation of formaldehyde, but then the adsorption energy should be strong enough to keep the methoxy group at the surface of the catalyst during its reaction with two methanol molecules which leads to formation of DMM.

6 Conclusions

In present work two major synthetic approaches, the electrochemical synthesis and the reaction of interaction between heptoxide of Rhenium and alkoxide complexes of Niobium and Tantalum were applied. Both approaches were successfully used for preparation of new mono-, bi- and trimetallic complexes and materials based on the Re, Nb and Ta, which are attractive for application as catalysts for different organic reactions.

The electrochemical synthesis based on the anodic dissolution of Rhenium metal in absolute EtOH turned out to be successful for the synthesis of $Re_4O_4(OEt)_{12}$ complex with the yields of the crystalline product about 70-80% (*see Fig. 21*).

The interaction of Re_2O_7 and ethoxide complexes with the common formula $M_2(OR)_{10}$ (M=Nb, Ta; R=Et, ^nPr) led successfully to the preparation of bimetallic $Nb_4O_2(OR)_{14}(ReO_4)_2$ (R=Et, ^nPr) and $Ta_4O_2(OEt)_{14}(ReO_4)_2$ oxoethoxo complexes with as high yield of the bulk products as 83, 88 and 86% respectively (*see Fig. 21*).

Due to isomorphous substitution for Niobium atoms by Tantalum ones it is possible to obtain by addition of Re_2O_7 the trimetallic oxomethoxo complexes with the common formula $(Nb_{1-x}Ta_x)_4O_2(OR)_{14}(ReO_4)_2$, where x = 0.3, 0.5, 0.4, 0.7 (R=Me, Et) with high yields (91, 90, 92, 91% respectively). The distribution of Nb and Ta is even at Nb:Ta = 1:1 but is a subject of considerable variation for the Nb- and Ta-rich samples, respectively (*see Fig. 21*).

The influence of the increase in the size of the alkoxide ligand and the metal ratios in the heterometallic species on the structure and properties of

the alkoxide precursors and the oxide materials produced from them has been established.

Nanosized particles about 3 nm in size of metallic Rhenium were successfully obtained via thermal decomposition of $Re_4O_4(OEt)_{12}$ in dry N_2 atmosphere at low temperatures (*see Fig. 21*).

The thermal decomposition in air of all the studied methoxide complexes $(Nb_{1-x}Ta_x)_4O_2(OMe)_{14}(ReO_4)_2$ (x = 0.3, 0.5, 0.7) leads to solid solutions with the structures related to the block crystal structure of the L–modification of Ta_2O_5 at the temperatures < 1000°C with semi–ordered macro porous structures, where the size of pores lies in the range 100-250 nm. The thermal decomposition in dry nitrogen provides solid solutions with the structures related to block structure of the H–modification of Nb_2O_5 for the Niobium-rich precursors and the L–modification of Ta_2O_5 for Ta:Nb ≥ 1:1 at the temperature < 1000°C (*see Fig. 21*).

Nanobeads were successfully obtained by both natural and accelerated hydrolysis, where the application of perrhenate as structure-directing ligand permits reproducible preparation of spherical particles conserving all of its Re content. The particles remain amorphous and retain Re until 700 °C, most probably due to formation of dense oxide layer on their surface. The Re content is lost at 1000 °C with formation of pores on the surface nanobeads with related to the block structure of the L–modification of Ta_2O_5 from $Ta_4O_2(OEt)_{14}(ReO_4)_2$ and $(Nb_{0.6}Ta_{0.4})_4O_2(OEt)_{14}(ReO_4)_2$, while from $Nb_4O_2(OR)_{14}(ReO_4)_2$ (R = Et, ^nPr) leads to formation H–modification of Nb_2O_5.

The application of alkoxide molecular precursors permits the creation of new rhenium and chemically connected rhenium-tantalum catalysts on mesoporous TiO_2 supports. The materials were obtained in ambient atmosphere with subsequent calcination at a relatively low temperature of 300 °C for 2h leading to crystalline products. The selectivity of rhenium oxide catalysts was mostly toward formaldehyde, but in the case of rhenium–tantalum oxide ones the major product of the methanol oxidation was DMM. The simultaneous presence of the chemically connected oxidative (perrhenate) and acidic (tantalum oxide) components in the catalyst apparently permit one-step production of DMM.
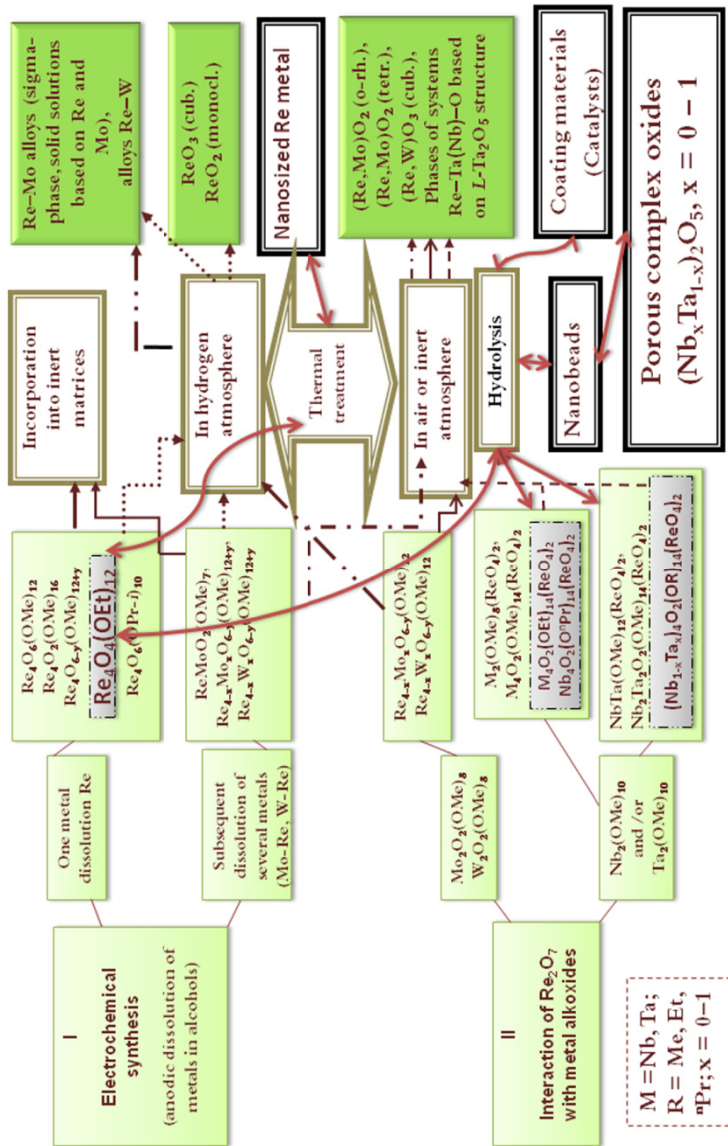
Figure 21. Scheme of preparation of the precursors and related materials

References

Anaya, S.A.S., Hagenbach, A. & Abram, U. (2008). Tricarbonylrhenium(I) and -technetium(I) complexes with bis(2-pyridyl)phenylphosphine and tris(2-pyridyl)phosphine. *Polyhedron* 27(18), 3587-3592.

ATOMS (2006). Version: 6.3. Kingsport, USA: Shapesoftware Inc.

Bakala, P.C., Briot, E., Millot, Y., Piquemal, J.-Y. & Bregeault, J.-M. (2008). Comparison of olefin metathesis by rhenium-containing – alumina or silica–aluminas and by some mesoporous analogues. *Journal of Catalysis* 258(1), 61-70.

Baruwati, B. & Varma, R.S. (2010). Synthesis of monodispersed tantalum (V) oxide nanospheres by ethylene glycol mediated route. *Crystal Growth & Design* 10, 3424-3428.

Bayot, D., Degand, M. & Devillers, M. (2005). Synthesis and characterization of homo- and heterobimetallic niobiumV and tantalumV peroxo-polyaminocarboxylato complexes and their use as single or multiple molecular precursors for Nb-Ta mixed oxides. *Journal of Solid State Chemistry* 178(9), 2635-2642.

Beattie, I.R., Gilson, T.R. & Jones, P.J. (1996). Vapor Phase Vibrational Spectar for Re_2O_7 and the Infrared Spectrum of Gaseous $HReO_4$. Molecular Spapes of Mn_2O_7, Tc_2O_7, and Re_2O_7 *Inorg. Chem.* 35, 1301-1304.

Brandhorst, M., Cristol, S., Capron, M., Dujardin, C., Vezil, H., Lebourdon, G. & Payen, E. (2006). Catalytic oxidation of methanol on Mo/Al_2O_3 catalyst: An EPR and raman/infrared operando spectroscopies study. *Catalysis Today* 113, 34-39.

Briand, L.E., Farneth, W.E. & Wachs, I.E. (2000). Quantitative determination of the number of active surface sites and the turnover frequencies for methanol oxidation ove metal oxide catalysts: I. Fundamentals of the methanol chemisorption technique and application to monolayer supported molybdenum oxide catalysts. . *Catalysis Today* 62, 219.

Budoace, S., Cimpeanu, V., Parvulescu, V., Centeno, M.A., Grange, P. & Parvulesku, V.I. (2004). Chemoselective oxidation of 2-thiomethyl-

4,6-dimethyl-pyrimidine on nanostructured tantalum oxides. *Catalysis Today* 91-92, 219-223.

Buffon, R., Auroux, A., Lefebvre, F., Leconte, M., Choplin, A. & Basset, J.-M. (1992a). A surface organometallic approach to the synthesis of rhenium-based catalysts for the metathesis of olefins: CH_3ReO_3/Nb_2O_5. *Journal of Molecular Catalysis* 76(1-3), 287-295.

Buffon, R., Choplin, A., Leconte, M. & Basset, J.-M. (1992b). Surface organometallic chemistry of rhenium: Attempts to characterize a surface carbene in metathesis of olefins with the catalysts CH_3ReO_3/Nb_2O_5. *Journal of Molecular Catalysis* 76(1-3), L7-L10.

Buffon, R., Jannini, M.J.D.M. & Abras, A. (1997). Effects of the addition of Nb_2O_5 to rhenium-based olefin metathesis catalysts. *Journal of Molecular Catalysis A: Chemical* 115(1), 173-181.

Camargo, E.R. & Kakihana, M. (2002). Low temperature synthesis of lithium niobate powders based on water-soluble niobium malato complexes. *Solid State Ionics* 151(1-4), 413-418.

Cecchet, F., Alebbi, M., Bignozzi, C.A. & Paolucci, F. (2006). Efficiency enhancement of the electrocatalytic reduction of CO_2: fac-[Re(v-bpy)(CO)$_3$Cl] electropolymerized onto mesoporous TiO_2 electrodes. . *Inorganica Chimica. Acta* 359(12), 3871-3874.

Chang, A.S.Y., Chen, W., Wang, H., Rowe, J.E. & Madey, T.E. (2004). Methanol reactions over oxygen-modified Re surfaces: Influence of Surface Structure and Oxidation. *Journal of Physical Chemistry B* 108(38), 14643-14651.

Chen, D.H., Huang, F.Z., Cheng, Y.B. & Caruso, R.A. (2009). Rhenium(I) tricarbonyl complexes with bispyridine ligands attached to sulfur-rich core: Synthesis, structure and properties. *Adv. Mater.* 21, 2206-2210.

Chen, Y., Fierro, J.L.G., Tanaka, T. & Wachs, I.E. (2003). Supported Tantalum Oxide Catalysts: Synthesis, Physical Charachterization, and Methanol Oxidation Chemical Probe Reaction *J. Phys. Chem. B.* 107, 5243-5250.

Chisholm, M.H., Folting, K., J.C.Huffman & Kirkpatrick, C.C. (1984). Reactions of metal-metal multiple bonds. reactions of $Mo_2(OR)_6$ and $[M(OR)_4]_x$ compounds with molecular oxygen. Preparation and characterization of oxo-alkoxides of Molybdenum of formula $MoO_2(OR)_2$, $MoO_2(OR)_2$(bpy), $MoO(OR)_4$, $Mo_3O(OR)_{10}$, $Mo_4O_8(OR)_4$(py)$_4$ and $Mo_6O_{10}(OR)_{12}$. . *Inorganic Chemistry* 23(8), 1021-1037.

Chisholm, M.H., Huffman, J.C., Kirkpatrick, C.C., Leonelly, J. & Folting, K. (1981). Metal alkoxides - models for metal oxides. Preparations and structures of hexadecaalkoxytetratungsten compounds, $W_4(OR)_{16}$, where R = Me and Et, and octaoxotetraisopropoxytetrapyridinotetramolybdenum,

$Mo_4(O)_4(\mu2-O)_2(\mu3-O)_2(OPr^i)_2(\mu2-OPr^i)2(py)_4$. . *Journal of the American Chemical Society* 103(20), 6093-6099.

Christoforou, A.M., Marilli, P.A., Fronczek, F.R. & Marzilli, L.G. (2007). fac-$[Re(CO)_3L]+$ complexes with N• CH_2• CH_2• X• CH_2• CH_2• N tridentate ligands. Synthetic, X-ray Crystallographic, and NMR spectroscopic investigations. *Inorganic Chemistry* 46(26), 11173-11182.

Cui, Y. & Jin, Z. (1999). Assessment of the Re-Ta binary system. *Journal of Alloys and Compounds* 285(1-2), 150-155.

Deligne, N., Bayot, D., Degand, M. & Devillers, M. (2007). Nb-Ta, Nb-Mo and Nb-V oxides prepared from hybrid organic-inorganic precursors. *Journal of Solid State Chemistry* 180(7), 2026-2033.

Dharmaraj, N., Park, H.C., Kim, C.H., Viswanathamurthi, P. & Kim, H.Y. (2006). Nanometer sized tantalum pentoxide fibers prepared by electrospinning. *Materials research Bulletin* 41, 612-619.

Dibenedetto, A., Pastore, C. & Aresta, M. (2006). Direct carboxylation of alcohols to organic carbonates: Comparison of the Group 5 element alkoxides catalytic activity: An insight into the reaction mechanism and its key steps. *Catalysis Today* 115(1-4), 88-94.

Doledec, G. & Commereuc, D. (2000). Synthesis and properties of homogeneous models of the Re_2O_7/Al_2O_3 metathesis catalyst. . *Journal of Molecular Catalysis A: Chemical* 161(1-2), 125-140.

Escalona, N., Ojeda, J., Cid, R., Alves, G., A.Lopez, A., Fierro, J.L. & Llambias, F.J.G. (2002). Characterization and reactivity of $Re_{(x)}/$ – Al_2O_3 catalysts in hydrodesulfurization and hydrodenitrogenation of gas oil: effect of Re loading. *Applied Catalysis A: General* 234(1-2), 45-54.

Escalona, N., Vrinat, M., Laureni, D. & Llambias, F.J.G. (2007). Rhenium sulfide in hydrotreating. . *Applied Catalysis A: General* 322, 113-120.

Esteves, A., Oliveira, L.C.A., Ramalho, T.C., Goncalves, M., Anastacio, A.S. & Carvalho, H.W.P. (2008). New materials based on modified synthetic Nb_2O_5 as photocatalyst for oxidation of organic contaminants. . *Catalysis Communications* 10(3), 330-332.

Feliczak, A., Walczak, K., Wawrzynczak, A. & Nowak, I. (2009). The use of mesoporous molecular sieves containing niobium for the synthesis of vegetable oil-based products. . *Catalysis Today* 140(1-2), 23-29.

George, G.N. & Pickering, I.J. (1993). *EXAFSPAK - A Suite of Computer Programs for Analysis of X-Ray Absorption Spectra*. Stanford, CA.

Gornay, J., Sécordel, X., Ménorval, B.d., Cristol, S., Fongarland, P., Capron, M., Duhamel, L., Payen, E., Dubois, J.-L. & Dumeignil, F. (2010). Direct conversion of methanol into 1,1-dimethoxymethane: remarkably high productivity over an FeMo catalyst placed under unsual conditions. *Green Chem.* 12(10), 1722-1725.

Guo, G. & Huang, J. (2011). Preparation of mesoporous tantalum oxide and its enhanced photocatalytic activity. *Materials Letters* 65, 64–66.

Guo, H., Li, D., Jiang, D., Li, W. & Su, Y. (2010). Characterization and performance of sulfated VO_x-TiO_2 catalysts in the one-step oxidation of methanol to dimethoxymethane. *Catalysis Communications* 11, 396–400.

Guryev, Y.V., Ivanova, I.I., Lunin, V.V., Grünert, W. & Berg, M.V.E.v.d. (2007). Characterization of metal segregation in Pt-Re/Al_2O_3 reforming catalysts. *Applied Catalysis A: General* 329, 16-21.

Halbritter, J. (1987). On the oxidation and on the superconductivity of niobium. . *Applied Physics A: Materials Science & Processing* 43(1), 1-28.

Held, A. & Florczak, P. (2009). Fischer-Tropsch synthesis on ceramic monolith-structured catalysts. *Catalysis Today* 142(3-4), 329-334.

Herrmann, W.A., Kühn, F.E., Fischer, R.W., Thiel, W.R. & Romao, C.C. (1992). Multiple bonds between main-group elements and transition metals. Simple and efficient synthesis of methyltrioxorhenium(VII): a general method. . *Inorganic Chemistry* 31(21), 4431-4432.

Ho, S.F., Contarini, S. & Rabalais, J.W. (1987). Ion-Beam-Induced Chemical Changes in the Oxyanions (MO-) and Oxides (MO), Where M = Cr, Mo, W, V, Nb, and Ta. *J. Phys. Chem.* 91, 4779-4788.

Hubert-Pfalzgraf, L.G., Pinkerton, A.A. & Riess, J.G. (1978). Structural and stereodynamic studies on molecular early transition metal derivatives. Synthesis, crystal structure, and molecular constitution of solutions of bis(alkoxo)trichloroniobium(V)-hexamethylphosphortriamide adducts. . *Inorganic Chemistry* 17(3), 663-667.

Hubert-Pfalzgraf, L.G. & Riess, J.G. (1975). Isolation of a mixed niobium tantalum alkoxide. . *Inorganic Chemistry* 14(11), 2854-2856.

Jain, K.R. & Kühn, F.E. (2007). Immobilization of organorhenium(VII) oxides. . *Journal of Organometallic Chemistry* 692(25), 5532-5540.

Jehng, J.-M., Tung, W.-C., Huang, C.-H. & Wachs, I.E. (2007). Structural characteristics and reactivity properties of the tantalum modified mesoporous silicalite (MCM-41) catalysts. . *Microporous Mesoporous Materials* 99(3), 299-307.

Johansson, K.E., Palm, T. & Werner, P.E. (1980). An automatic microdensitometer for X-ray powder Diffraction Photographs. *Journal of Physics E: Scientific Instruments* 13(12), 1289-1291.

Katou, T., Lu, D., Kondo, J.N. & Domen, K. (2002). Synthesis of 2D-hexagonally ordered mesoporous niobium and tantalum mixed oxide. . *Journal of Materials Chemistry* 12(5), 1480-1483.

Kessler, V.G. (2009). *J. Sol-Gel Sci. Tech.* 51, 264-271.

Kessler, V.G., Shevelkov, A.V., Kvorykh, G.V., Seisenbaeva, G.A., Turova, N.Y. & Drobot, D.V. (1995). Electrochemical synthesis and physicochemical properties of rhenium(V) oxomethoxide $Re_4O_2(OMe)_{16}$. . *Russian Journal of Inorganic Chemistry* 40(9), 1477-1479.

Kessler, V.G., Spijksma, G.I., Seisenbaeva, G.A., Håkansson, S., Blank, D.H.A. & Bouwmeeter, H.J.M. (2006). New insight in the role of modifying ligands in the sol-gel processing of metal alkoxide precursors: A possibility to approach new classes of materials. *J. Sol-Gel Sci. Tech.* 40, 163-179.

Kirihara, M., Yamamoto, J., Noguchi, T. & Hirai, Y. (2009). Selective synthesis of sulfoxides and sulfones by tantalum(V) catalyzed oxidation of sulfides with 30% hydrogen peroxide. . *Tetrahedron Letters* 50(11), 1180-1183.

Kondo, J.N., Yamashita, T., Katou, T., Lee, B., Lu, D., Hara, M. & Domen, K. (2002). Single crystal particles of mesoporous $(Nb,Ta)_2O_5$. *Studies in Surface Science and Catalysis* 141, 265-272.

Kusakari, T., Sasaki, T. & Iwasawa, Y. (2004). Selective oxidation of benzene to phenol with molecular oxygen on rhenium/zeolite catalysts. . *Chemical Communications* (8), 992-993.

Kustov, A.L., Kessler, V.G., Romanovsky, B.V., Seisenbaeva, G.A., Drobot, D.V. & Shcheglov, P.A. (2004a). Nanomaterials prepared from Re-Mo oxomethoxide binuclear complexes and zeolites: Synthesis and Physicochemical properties. *Russian Journal of Physical Chemistry A, Focus on Chemistry* 78(1), S63-S67.

Kustov, A.L., Kessler, V.G., Romanovsky, B.V., Seisenbaeva, G.A., Drobot, D.V. & Shcheglov, P.A. (2004b). Supported Re and Mo oxides prepared using binuclear precursors: synthesis and characterization. . *Journal of Molecular Catalysis A: Chemical* 216(1), 101-106.

Laurenti, D., Thi, K.T.N., Escalona, N., Massin, L., Vrinat, M. & Llambias, F.J.G. (2008). Support effect with rhenium sulfide catalysts. . *Catalysis Today* 130(1), 50-55.

Lee, B.J., Yamashita, T., Lu, D.L., Kondo, J.N. & Domen, K. (2002). Single-Crystal particles of mesoporous Niobium• Tantalum mixed oxide. *Chemistry of Materials* 14(2), 867-875.

Lin, K.L. & Wang, H.C. (1988). Hydrolysis of zirconium alkoxide under an uncontrolled atmosphere. *J. Mater. Sci.* 23, 3666-3670.

Liu, Z.-K. & Chang, Y.A. (2000). Evaluation of the thermodinamic properties of the Re-Ta and Re-W systems. . *Journal of Alloys and Compounds* 299(1-2), 153-162.

Lufaso, M.W., Schulze, W.A., Misture, S.T. & Vanderah, T.A. (2007). Crystal structure, magnetic, and dielectric properties of Aurivillius-type $Bi_5Fe_{0.5}Nb_{1.5}O_9$. . *Journal of Solid State Chemistry* 180(10), 2655-2660.

Malmros, G. & Werner, P.E. (1973). SCANPY, 493-502.

Mandelli, D., Vliet, M.C.A.v., Arnold, U., Sheldon, R.A. & Schuchardt, U. (2001). Epoxidation of alkenes with hydrogen peroxide catalyzed by $ReO_4^-SiO_2 \cdot Al_2O_3$ and $ReO_4-Al_2O_3$. *Journal of Molecular Catalysis A: Chemical* 168(1-2), 165-171.

Masse, J.-P., Szymanowski, H., Zabeida, O., Amassian, A., Klemberg-Sapieha, J.E. & Martinu, L. (2006). Stability and effect of annealing on the optical properties of plasma-deposited Ta_2O_5 and Nb_2O_5 films. . *Thin Solid Films* 515(4), 1674-1682.

Matsuoka, Y., Nywa, M. & Murakami, Y. (1990). Morphology of molybdena supported on varios oxides and iits activity for methanol oxidation. *J. Phys. Chem.* 94, 1477-1482.

Mealli, C. & Proserpio, D.M. (1990). MO theory made visible (CS). *Journal of Chemical Education* 67, 339-402.

Mohammed, M.R. & Sherman, W.F. (1981). Infrared and Raman spectra of ReO_4^- isolated in alkali halides of CsCl structure. *J. Phys. C.: Solid State Phys.* 14, 4121-4130.

Mohanty, G.P., Fiegel, L.J. & Healy, J.H. (1964). On the system Niobium pentoxide - Tantalum pentoxide. . *Journal of Physical Chemistry B* 68(1), 208-210.

Mol, J.C. (2004). Catalytic metathesis of unsaturated fatty acid esters and oils. . *Topics in Catalysis* 27(4), 97-104.

Mugishima, T., Yamada, M. & Yoshinari, O. (2006). Study of hydrogen diffusion in Nb-Ta alloys by Gorsky effect measurement. . *Materials Science and Engineering A* 442(1-2), 119-123.

Muthurajan, H., Kumar, H.H., Rao, N.K., Pradhan, S., Jha, R.K. & Ravi, V. (2008). Low temperature synthesis of $SrNb_2O_6$ and $SrTa_2O_6$ using hydroxide precursor. *Materials Letters* 62(6-7), 892-894.

Nakajima, K., Lu, D., Hara, M., Domen, K. & Kondo, J.N. (2005). Synthesis and application of thermally stable mesoporous Ta_2O_5 photocatalyst for overall water decomposition. . *Studies in Surface Science and Catalysis* 158, 1477-1484.

Naor, A., Eliaz, N., Burstein, L. & Gileadi, E. (2010). Direct Expiremental Support for the Catalytic Effect of Iron-Group Metals on Electrodeposition of Rhenium *Electrochemical and Solid-State Letters* 13(12), D91-D93.

Oikawa, T., Oosohi, T., T.Tanaka, Yamamoto, T. & M.Onaka (2004). A new heterogeneous olefin metathesis catalyst composed of rhenium oxide and mesoporous alumina. *Microporous Mesoporous Materials* 74, 93-103.

Okal, J. (2005). A study of effect of particle size on the oxidation of rhenium in the Re/ -Al_2O_3 catalysts. *Applied Catalysis A: General* 287(2), 214-220.

Okal, J. & Kubicka, H. (1998). Influence of oxidation-reduction treatment on activity and selectivity of Re supported on -alumina. *Applied Catalysis A: General* 171(2), 351–359.

Onaka, M. & Oikawa, T. (2002). Olefin Metathesis over Mesoporous Alumina-supported Rhenium Oxide Catalyst. *Chemistry Letters* 31(8), 850–851.

Prado, A.G.S., Bolzon, L.B., Pedroso, C.P., Moura, A.O. & Costa, L.L. (2008). Nb_2O_5 as efficient and recyclable photocatalyst for indigo carmine degradation. . *Applied Catalysis B: Enviromental* 82(3-4), 219-224.

Robin, A. & Rosa, J.L. (2000). Corrosion behavior of niobium, tantalum and their alloys in hot hydrochloric and phosphoric acid solutions. . *International Journal of Refractory Metals and Hard Materials* 18(1), 13-21.

Rosenfield, D., Schmid, P.E., Szeles, S., Levy, F., Demarne, V. & Grisel, A. (1996). Electrical transport properties of thin-film metal-oxide-metal Nb_2O_5 oxygen sensors. . *Sensors and Actuators, B: Chemical* 37(1-2), 83-89.

Royer, S., Sécordel, X., Brandhorst, M., Dumeignil, F., Cristol, S., Dujardin, C., Capron, M., Payen, E. & Dubois, J.-L. (2007). *Chem. Commun* 7, 865-867

Räty, J. & Pakkanem, T.A. (2000). Controlled gas phase preparation and HDS activity of $Re_2(CO)_{10}$ alumina catalysts. . *Catalysis Letters* 65(4), 175-180.

Saint-Arroman, R.P., Didillon, B., Mallmann, A., Basset, J.M. & Lefebvre, F. (2008). Deperoxidation of cyclohexyl hydroperoxide by silica-supported alkoxo-tantalum complexes. . *Applied Catalysis A: General* 337(1), 78-85.

Sairre, M.I.S., Bronze-Uhle, E.S. & Donate, P.M. (2006). Niobium(V) oxide: a new and efficient catalyst for the transesterification of -keto esters. *Tetrahedron Letters* 46(15), 2705-2708.

Salameh, A., Baudoin, A., Daravong, S., Boehm, V., Roeper, M., Basset, J.-M. & Coperet, C. (2008). CH_3-ReO_3 on -Al_2O_3: Activity, selectivity, active site and deactivation in olefin metathesis. *Journal of Catalysis* 253(1), 180-190.

Salameh, A., Joubert, J., Baudouin, A., Lukens, W., Delbecq, F., Sautet, P., Basset, J.M. & Coperet, C. (2007). CH_3ReO_3 on Y-Al_2O_3: Understanding its structure, initiation, and reactivity in olefin metathesis. *Angewandte Chemie International Edition* 18(21), 3870-3873.

Scheiring, T., Klein, A. & Klaim, W. (1997). EPR study of paramagnetic rhenium(I) complexes $[(bpy)Re(CO)_3]_x$ relevant to the mechanism of electrocatalytic CO2 reduction . *Perkin Transaction* 22(12), 2569-2572.

Secordel, X., Berrier, E., Capron, M., Cristol, S., Paul, J.-F., Fournier, M. & Payen, E. (2010). TiO_2-supported rhenium oxide catalysts for methanol oxidation: Effect of support texture on the structure and reactivity evidenced by an operando Raman study. *Catalysis Today* 155, 177-183.

Seisenbaeva, G.A., Baranov, A.I., Shcheglov, P.A. & Kessler, V.G. (2004). Isolation, X-ray single crystal and theoretical study of quinquevalent metal oxoisopropoxides, $Nb_6O_8(^iPrO)_{14}(^iPrOH)_2$ and $Re_4O_6(O^iPr)_{10}$. *Inorganica Chimica Acta* 357(2), 468-474.

Seisenbaeva, G.A. & Kessler, V.G. (2001). Perrhenate ligand as an analog of the methoxide group in alkoxide complexes. Synthesis and X-ray single crystal study of $Ta_2(OMe)_8(ReO_4)_2$. *Inorganic Chemistry Communication* 4(10), 534-536.

Seisenbaeva, G.A., Kessler, V.G., Pazik, R. & Strek, W. (2008). Heteroleptic metal alkoxide "oxoclusters" as molecular models for the sol-gel synthesis of perovskite nanoparticles for bio-imaging applications. *Dalton Transact.* (26), 3412-3421.

Seisenbaeva, G.A., Moloney, M.P., Tekoriute, R., Hardy-Dessource, A., Nedelec, J.M., Gun'ko, Y.K. & Kessler, V.G. (2010). Biometric synthesis of hierarchically porous nanostructured metal oxide microparticles - potential scaffolds for drug delivery and catalysis. *Langmuir* 26(12), 9809-9817.

Seisenbaeva, G.A., Shevelkov, A.V., Kloo, L., Gohil, S., Tegenfeldt, J. & Kessler, V.G. (2001). Homo- and hetero-metallic rhenium oxomethoxide complexes with a $M_4(\mu-O)_2(\mu-OMe)_4$ planar core-a new family of metal alkoxides displaying a peculiar structural disorder. Preparation and X-ray single crystal study. . *Dalton Transactions* 19, 2762-2768.

Shannon, R.D. (1976). Revised effective ionic radii and systematic studies of interatomic distances in halides and chalcogenides. *Acta Crystollagraphica A* 32(5), 751-767.

Shcheglov, P.A., Seisenbaeva, G.A., Drobot, D.V. & Kessler, V.G. (2001). The electrochemical synthesis and X-ray single crystal study of $Re_4O_6(O^iPr)_{10}$ - a new Rhenium(V, VI) cluster with an unprecedented arrangement of metal-metal bonds. . *Inorganic Chemistry Communication* 4(5), 227-229.

Shcheglov, P.A., Seisenbaeva, G.A., Gohil, S., Drobot, D.V. & Kessler, V.G. (2002). Preparation of trimetallic alkoxide complexes exploiting the isomorphous substitution approach. Synthesis, X-ray single crystal and mass-spectrometric study of $NbTa(OMe)_8(ReO_4)_2$ and $Nb_2Ta_2O_2(OMe)_{14}(ReO_4)_2$. *Polyhedron* 21, 2317-2322.

SHELXTL-NT (1998). *SHELXTL-NT Reference Manual*. Madison: WI.

Shirley, D.A. (1972). Magnetoplasma surface waves in metals. . *Phys. Rev. B* 5(12), 4709.

Shu, Y., Ohnishi, R. & Ichikawa, M. (2003). Improved methane dehydrocondensation reaction on HMCM-22 and HZSM-5 supported rhenium and molybdenum catalysts. *Applied Catalysis A: General* 252, 315-329.

Sobczac, I., Kieronczyk, N., Trejda, M. & Ziolek, M. (2008). Gold, vanadium and niobium containing MCM-41 materials-Catalytic properties in methanol oxidation. *Catalysis Today* 139(3), 188-195.

Stodolny, M. & Laniecki, M. (2009). Synthesis and characterization of mesoporous Ta_2O_5-TiO_2 photocatalysts for water splitting. . *Catalysis Today* 142(3-4), 314-319.

Tanabe, K. (2003). Catalytic application of niobium compounds. . *Catalysis Today* 78(1-4), 65-77.

Tatibouët, J.-M. (1997). Methanol oxidation as a catalytic surface probe. *Appl. Catal. A : General* 148, 213-252.

Thompson, A., Attwood, D., Gullikson, E., Howells, M., Kim, K.-J., Kirz, J., Kortright, J., Lindau, I., Pianatta, P., Robinson, A., Scofield, J., Underwood, J., Vaughan, D., Williams, G. & Winick, H. (2001). *X-ray Data Booklet*. Berkeley, California 94720.

Trejda, M., Kujawa, J., Ziolek, M. & Mrowiec-Bialon, J. (2008). Nb-containing mesoporous materials of MCF type-Acidic and oxidative properties. *Catalysis Today* 139(3), 196-201.

Truijen, I., Haeldermans, I., Bael, M.K.v., Rul, H.v.d., Haen, J.D., Mullens, J., Terryn, H. & Goossens, V. (2007). Influence of synthesis parameters on morphology and phase composition of porous titania layers prepared via water based chemical solution deposition. *Journal of the European Ceramic Society* 27(16), 4537-4546.

Tsoncheva, T., Vankova, S., Bozhkov, O. & Mehandjiev, D. (2007). Rhenium and manganese modified activated carbon as catalyst for methanol decomposition. *Canadian Journal of Chemistry* 85(2), 118-123.

Turevskaya, E.P., Turova, N.Y., Korolev, A.V., Yanovsky, A.I. & Struchkov, Y.T. (1995). Bimetallic alkoxides of Niobium. *Polyhedron* 14, 1531-1542.

Turova, N.Y., Korolev, A.V., Tchebukov, D.E., Belokon, A.I., Yanovsky, A.I. & Struchkov, Y.T. (1996). Tantalum(V) alkoxides : Electrochemical synthesis, mass-spectral investigation and oxoalkoxocomplexes. . *Polyhedron* 15(21), 3869-3880.

Turova, N.Y., Turevskaya, E.P., Kessler, V.G. & Yanovskaya, M.I. (Eds.) (2002). *The Chemistry of Metal Alkoxides.*: Boston, Dordrecht, London: Kluwer Academic Publishers.

Ushikubo, T. (2000). Recent topics of research and development of catalysis by niobium and tantalum oxides. *Catalysis Today* 57(3-4), 331-338.

Wang, L., Murata, K. & Inaba, M. (2003). Production of pure hydrogen and more valuable hydrocarbons from ethane on a novel highly

active catalyst system with a Pd-based membrane reactor. . *Catalysis Today* 82(1-4), 99-104.

Wang, L., Ohnishi, R. & Ichikawa, M. (2000). Selective Dehydroaromatization of Methane toward Benzene on Re/HZSM-5 Catalysts and Effects of CO/CO_2 Addition. *Journal of Catalysis* 190(2), 276-283.

Vinet, B., Benoit, M., Touet, I. & Drevet, B. (2003). Undercooling experiments on niobium–rhenium alloys from drop-tube processing. *Scripta Materialia* 48(9), 1391-1396.

Wright, D.A. & Williams, D.A. (1968). The crystal and molecular structure of titanium tetramethoxide. *Acta Crystallographica* 24(8), 1107-1114.

Xiao, J. & Puddephatt, R.J. (1995). Pt-Re clusters and bimetallic catalysts. *Coordination Chemistry Reviews* 143, 457-500.

Xu, L., Yang, X., Yu, X. & Guo, Y. (2008). Preparation of mesoporous polyoxometalate–tantalum pentoxide composite catalyst for efficient esterification of fatty acid. *Catalysis Communications* 9(7), 1607-1611.

Yang, P., Deng, T., Zhao, D., Feng, P., Pine, D., Chmelka, B., Whitesides, G. & Stucky, G. (1998). Hierarchically Ordered Oxides. *Science* 282, 2244-2246.

Yuan, Y. & Iwasawa, Y. (2002). Performance and Characterization of Supported Rheniu Oxide catalysts for Selective Oxidation of Methanol to Methylal. *J. Phys. Chem. B* 106, 4441-4449.

Yuan, Y., Liu, H., Imoto, H., Shido, T. & Iwasawa, Y. (2000a). Performance and Caharacteriization of a New crystalline SbRe2O6 Catalyst for Selective Oxidation of Methanol to methylal. *Journal of Catalysis* 195, 51-61.

Yuan, Y., Shido, T. & Iwasawa, Y. (2000b). The new catalytic property of supported rhenium oxides for selective oxidation of methanol to methyl. *Chemical Communications* 15, 1421-1422.

Yue, Y. & Gao, Z. (2000). Synthesis of mesoporous TiO_2 with a crystalline framework. . *Chemical Communications* 18, 1755-1756.

Zhao, H., Bennici, S., Shen, J. & Auroux, A. (2010). Nature of surface sites of V_2O_5-TiO_2/SO_4^{2-} catalysts and reactivity in selective oxidation of methanol to dimethoxymethane. *Journal of Catalysis* 272, 176-189.

Zou, Z.G., Arakawa, H. & Ye, J.H. (2002). Substitution effect of Ta^{5+} by Nb^{5+} on photocatalytic, photophysical, and structural properties of $BiTa_{1-x}Nb_xO_4$ (0 – 1.0). . *Journal of Materials Research* 17(6), 1446-1454.

Acknowledgments

It is a pleasure to thank the many people who made this thesis possible.

First and foremost I would like to thank my advisor **Gulaim Seisenbaeva**. It has been an honor to be her first Ph.D. student. She has taught me, both consciously and un-consciously, how good experimental chemistry is done. I appreciate all her contributions of time, ideas, and funding to make my Ph.D. experience productive and stimulating. The joy and enthusiasm she has for her research was contagious in forming my motivation, even during tough times in the pursuit of my Ph.D. degree. I am also thankful for the excellent example she has provided as a successful female chemist and future professor.

I am deeply grateful to my assistant supervisor **Vadim Kessler**, for his detailed and constructive comments, and for his important support throughout this work.

Also, I would like to thank my other assistant supervisor **Margareta Sundberg**, for her help and support.

I wish to express my warm and sincere thanks to **Mickael Capron**, who introduced me to the field of selective oxidation catalysis and for his thoughtful collaboration, which resulted in our first common article with great results.

I warmly thank **Elena Ossipova, Robert Pazik and Kai Wilkinson**, for their valuable advices and friendly help. Their extensive discussions around my work and interesting explorations in operations have been very helpful for this study.